NACA RM E52B12

NACA

RESEARCH MEMORANDUM

IMPINGEMENT OF WATER DROPLETS ON AN NACA 65_1-212 AIRFOIL AT AN ANGLE OF ATTACK OF 4°

By Rinaldo J. Brun, John S. Serafini
and George J. Moshos

Lewis Flight Propulsion Laboratory
Cleveland, Ohio

NATIONAL ADVISORY COMMITTEE
FOR AERONAUTICS

WASHINGTON
September 10, 1952

(4)

Release Date
12-11-52

ERRATA NO. 1

NACA RM E52B12

IMPINGEMENT OF WATER DROPLETS ON AN NACA 65_1-212 AIRFOIL AT AN ANGLE OF ATTACK OF 40°

By R. J. Brun, J. S. Serafini, and G. J. Moshos

September 16, 1952

The ordinate values in figure 3 of this report should be divided by 10.

NATIONAL ADVISORY COMMITTEE FOR AERONAUTICS

RESEARCH MEMORANDUM

IMPINGEMENT OF WATER DROPLETS ON AN NACA 65_1-212 AIRFOIL AT AN ANGLE OF ATTACK OF 4°

By Rinaldo J. Brun, John S. Serafini, and

George J. Moshos

SUMMARY

The trajectories of droplets in the air flowing past an NACA 65_1-212 airfoil at an angle of attack of 4° were determined. The collection efficiency, the area of droplet impingement, and the rate of droplet impingement were calculated from the trajectories and are presented herein to cover the following range of conditions:

Variable	Minimum value	Maximum value
Droplet diameter (microns)	5	100
Airplane speed (mph)	150	Critical flight speed
Altitude (ft)	1000	35,000
Chord length (ft)	2	20

INTRODUCTION

As part of a comprehensive research program directed toward an appraisal of the problem of ice prevention on high-speed aircraft, an investigation of the impingement of cloud droplets on airfoils and other aerodynamic bodies has been undertaken at the NACA Lewis laboratory. The investigation includes a study of the extent of impingement on a low-drag airfoil and the rate of droplet impingement per unit area of the airfoil area affected. Previous investigators have calculated the water-droplet trajectories for cylinders (references 1 and 2) and for Joukowski airfoils (references 3 and 4). An empirical method for determining area, rate, and distribution of water-droplet impingement on airfoils of arbitrary sections is presented in reference 5. The method is more firmly established for 15-percent-thick airfoils resembling Joukowski airfoil sections than for low-drag airfoils, because the basic data used in developing the empirical method were obtained for four Joukowski airfoil sections and only one low-drag section. Further water-droplet trajectory data are needed for low-drag airfoils and particularly for airfoil sections thinner than the 15-percent-thick sections for which results are reported in the references cited.

The studies presented in this report are for an NACA 65_1-212 airfoil, which is a 12-percent-thick wing, placed at an angle of attack of 4°. The NACA 65-series airfoil sections are particularly adaptable to airplanes having high-level flight speeds. An airfoil 12 percent thick was chosen as adaptable to transport and cargo airplanes. An angle of attack of 4° was chosen as being representative of low cruise attitude for a turbojet-powered aircraft operated under conditions giving a relatively large area of droplet impingement on the airfoil. The results presented herein are applicable to the NACA 65_1-212 airfoil under the following conditions: chord lengths from 2 to 20 feet; altitudes from 1000 to 35,000 feet; airplane speeds from 150 miles per hour to the critical flight Mach number; and droplet diameters from 5 to 100 microns.

ANALYSIS

As an airfoil moves through a cloud, the interception of the cloud droplets by the airfoil is dependent on the physical configuration of the airfoil and on the inertia of the cloud droplets. In order to obtain the extent of impingement and the rate per unit area of droplet impingement on an airfoil, the cloud droplet trajectories with respect to the airfoil must be determined. The differential equations that describe the droplet motion have been stated in reference 2 and are presented herein in the following form:

$$\left.\begin{aligned} \frac{dv_x}{d\tau} &= \frac{C_D Re}{24}\frac{1}{K}(u_x - v_x) \\ \frac{dv_y}{d\tau} &= \frac{C_D Re}{24}\frac{1}{K}(u_y - v_y) \end{aligned}\right\} \tag{1}$$

where

$$K \equiv \frac{2}{9}\frac{\rho_w a^2 U}{\mu L} \tag{2}$$

and

$$\left(\frac{Re}{Re_0}\right)^2 = (u_x - v_x)^2 + (u_y - v_y)^2 \tag{3}$$

(All symbols are defined in appendix A.) The dimensions of the free-stream velocity U in equation (2) are feet per second in order that the dimensions of the other variables in the equation be consistent with the definitions given in the list of symbols.

The differential equations (1) state that the motion of a droplet is governed by the drag forces imposed on the droplet by the relative motion between the droplet and the air moving along the streamlines around the airfoil. The droplet momentum tends to keep the droplet moving in a straight path, while the drag forces tend to force the droplet to follow the streamlines. For very small droplets and slow speeds, the momentum of the droplets parallel to the direction of the free-stream motion is small and the drag forces are large enough that little deviation from the streamlines occurs; whereas for large droplets and high speeds, the momentum is great enough to cause the droplets to deviate from the streamlines. In accordance with equations (1) and the definition of the parameter K in equation (2), for a given size and configuration of airfoil, the trajectories depend on the radius of the droplets, the airspeed, and the air viscosity as first-order variables. The trajectories also depend on the physical configuration of the airfoil and its angle of attack, in that these two variables determine the magnitude of the component velocities of the air u_x and u_y everywhere in the flow field.

The component air velocities were determined by a vortex substitution method that requires a knowledge of the pressure distribution on the surface of the airfoil. The pressure distribution was obtained from wind-tunnel data taken at the Ames laboratory. The method for calculating the local perturbation velocities in the two-dimensional incompressible flow field ahead of the airfoil is described in part in reference 6 and is presented more fully in appendix B. The computations were performed with electronic calculating machines employing punched cards. An incompressible flow field was obtained with the vortex substitution method. Preliminary calculations showed that the effect of compressibility of air on the trajectories of droplets was not a first-order effect up to the critical Mach number of the airfoil. Because of these preliminary calculations, the results presented herein are applicable up to the flight critical Mach number.

The more important assumptions that have been necessary in order to solve the problem are:

(1) At a large distance ahead of the airfoil (free-stream conditions) the droplets move with the same velocity as the air.

(2) The droplets are always spherical and do not change in size.

(3) No gravitational force acts on the droplets.

METHOD OF SOLUTION

The differential equations of motion (equation (1)) are difficult to solve by ordinary means because the values of the velocity components of the air and the term containing the coefficient of drag are not known until the trajectory is traced. These values are determined as the trajectory of a droplet is developed because the magnitudes depend on the position of the droplet in the flow field. Simultaneous solutions for the two equations were obtained with the use of a mechanical analog constructed at the Lewis laboratory for this purpose. The answers were obtained in the form of plots of the droplet trajectories with respect to the airfoil. The coefficient of drag C_D for the droplets, required in equations (1), was obtained from tables in references 2 and 3.

The equations of motion (equations (1)) were solved for the following six values of the parameter K: 1/100, 1/50, 1/10, 1/5, 1, and 2. For each value of the parameter K a series of trajectories was computed for each of three values of free-stream Reynolds number Re_0 (16, 256, and 1024). (A graphical procedure for interpreting the dimensionless parameters used in this report in terms of airplane speed, chord length, altitude, and droplet size is presented in appendix C.) Each series of trajectories encompassed the airfoil with a trajectory that was tangent to the upper surface of the airfoil and with a trajectory that was tangent to the lower surface of the airfoil. The upper and lower tangent trajectories started at free-stream conditions at distances $y_{0,u}$ and $y_{0,l}$, respectively, below the geometric chord line of the airfoil (fig. 1). The geometric chord line of the airfoil is oriented to coincide with the x-axis of the rectangular coordinate system, and the leading edge is placed at the origin of the coordinates. At an infinite distance ahead of the airfoil, the uniform air flow carrying the cloud droplets is assumed to be approaching the airfoil from the negative x-direction at an angle of 4° with respect to the geometric chord line. All distances are dimensionless because they are ratios to the airfoil chord length L, which is assumed to be the unit of distance.

Before the integration of the equations of motion could be performed with the analog, the initial velocity and acceleration of the droplets had to be determined. As postulated in the assumptions, at an infinite distance ahead of the airfoil, all the droplets have vertical and horizontal components of velocities that are the same as those of the free-stream air. At finite distances ahead of the leading edge of the airfoil, the droplets have velocity components and positions varying between those pertaining to the free stream and to the streamlines. At 5 chord lengths ahead of the airfoil, the air streamlines were found to deviate from free-stream conditions by less than the expected accuracy of the analog; therefore this point was assumed to be a safe position to assign the initial conditions to the droplets as being those of the

air streamlines. Because the time required to trace each trajectory from 5 chord lengths ahead of the airfoil up to the airfoil surface was prohibitive, the plotting by the analog was started at 1 chord length ahead of the airfoil leading edge. The starting conditions at 1 chord length ahead of the leading edge were determined for each of the six values of K studied by calculating a sample trajectory that started at $x = -5$. A preliminary study showed that while a droplet is approaching a position 1 chord length ahead of the airfoil, the amount of deviation of the droplet trajectory from the air streamline on which the droplet had started depends only on the value of K and not on the starting value of y at $x = -5$, provided the value of y is within the region of interest in this problem. Because the sample trajectories for each value of K studied were calculated from $x = -5$ to $x = -1$ in order to determine the starting values of droplet velocity and y-ordinate at $x = -1$, the final results were the same as if each trajectory were calculated from 5 chord lengths ahead of the airfoil leading edge. A study also revealed that the assignment of either free-stream or streamline values to the droplets at $x = -1$ was not sufficiently accurate, because the trajectories from 1 chord length ahead of the airfoil surface are very sensitive to small variations in the droplet velocity starting conditions assigned at 1 chord length ahead of the airfoil.

RESULTS AND DISCUSSION

The series of trajectories computed for each combination of values of K and Re_0 studied permits the evaluation of the area, the rate, and the distribution of water-droplet impingement on the NACA 65_1-212 airfoil section at an angle of attack of 4°. The tangent trajectories determine the area, or extent, of impingement. All droplets having trajectories between the tangent trajectories will strike the airfoil, whereas all droplets having trajectories not bounded by the tangent trajectories will miss the airfoil. The tangent trajectories also determine the rate of over-all droplet impingement, because the amount of water-droplet impingement on the whole wing is governed by the spacing of the tangent trajectories ($y_{0,u} - y_{0,l}$, fig. 1) at a large distance ahead of the airfoil where the cloud is uniform. The manner in which all the droplets collected are distributed over the area of impingement is determined by the behavior of those trajectories that are bounded by the tangent trajectories.

The results are often presented herein as functions of the parameter K. The parameter K has been called the inertia parameter, because its magnitude directly reflects the external force required on a droplet to cause a deviation from its original line of motion. For large values of K (that is, $K > 1$) which correspond, for example, to

droplets larger than 50 microns in diameter moving toward a 6-foot-chord airfoil at 400 miles per hour, the droplet trajectories deviate by only small amounts from straight lines. For values of K less than 1/50 which correspond, for example, to droplets less than 12 microns in diameter moving at less than 300 miles per hour toward an airfoil section with a 12-foot chord, the droplet trajectories more nearly coincide with the air streamlines.

The results are also often presented in terms of the scale parameter

$$\psi \equiv \frac{Re_0}{K} = \frac{9L\,\rho_a}{a\,\rho_w} \tag{4}$$

where L and a must be in the same units. The parameter ψ is called a scale parameter, because at any given altitude the value of ψ varies directly as the ratio of the airfoil chord length to the droplet size. For a tapered wing, the ψ parameter permits the direct evaluation of the amount of spanwise droplet impingement on the wing, because the entire wing is subjected to droplets of the same size and to the same air and water densities. The chord length is the only spanwise variable appearing in the scale parameter. For each section of span considered, the taper must be small enough that two-dimensional flow over the section is approximated. The scale parameter also permits a direct comparison of the impingement that can be expected on an airfoil passing through numerous clouds each composed of droplets uniform in size in each cloud but varying in size from one cloud to another.

Rate of water interception. - In flight the total rate of water interception, in pounds of water per hour per foot of wing span, is determined both by the droplet trajectories and by the meteorological conditions. The liquid-water content, in grams per cubic meter, and the droplet size are the important meteorological conditions. The speed and the size of the airfoil, as well as the droplet size, affect the tangent droplet trajectories, which determine the droplets that strike the airfoil. The total rate of water interception per unit span of the airfoil on that portion of the airfoil surface bounded by the upper and the lower tangent trajectories (fig. 1) can be calculated from the information in figure 2 and the following relation:

$$W_m = 0.329\,(y_{0,u} - y_{0,l})\,LUw\cos\alpha \tag{5}$$

where the flight speed U is in miles per hour. Figure 2 is a plot of the spacing between the upper and the lower tangent trajectories at free-stream conditions as a function of the reciprocal of the inertia parameter.

The rate of water interception is decreased as $1/K$ is increased, particularly for values of $1/K$ larger than 1. An increase in Re_0 also decreases the rate of water interception. The values of $1/K = 21$ and $Re_0 = 187$ represent the conditions for an airfoil with a 12-foot chord traveling at 400 miles per hour through a cloud composed of droplets 17 microns in diameter at an altitude of 10,000 feet. The corresponding value for $y_{0,u} - y_{0,l}$ required for equation (5) is 0.022. If the same airfoil is considered in flight at 200 miles per hour (droplet size and altitude not varied), the values of $1/K$ and Re_0 change to 42 and 94, respectively, and the value of $y_{0,u} - y_{0,l}$ changes to 0.016, a decrease of 27 percent. The decrease in rate of water impingement (equation (5)) is 64 percent. The effect of speed on the rate of water impingement is large, because the spacing between the two tangent trajectories is affected by the speed and the speed appears directly in equation (5).

The variation of rate of water interception with airfoil speed is summarized for an altitude of 20,000 feet in figure 3, in which the ordinate W_m/w is the total rate of water impingement per foot span of airfoil per unit liquid-water content (g/cu m) in the cloud. The total rate of water impingement can be obtained as a product of the results in figure 3 and the liquid-water content existing in the cloud. Several chord lengths ranging in value from 2 feet to 20 feet have been considered in figure 3. The values in figure 3(a) are for flight through a uniform cloud composed of droplets 15 microns in diameter; and in figure 3(b), for 20 microns in diameter. As is shown herein, the effect of a change in altitude is a second-order variable; therefore, the results of figure 3 are applicable over a wide range of altitudes.

Collection efficiency. - The collection efficiency of an airfoil has been defined (references 3 and 4) as the ratio of the amount of water intercepted to the amount of water originally contained in a volume of cloud swept out by the airfoil when at zero geometric angle of attack. The collection efficiency

$$E_m = \frac{(y_{0,u} - y_{0,l}) \cos \alpha}{T}$$

is presented in figure 4 as a function of the scale parameter ψ. The preceding definition of collection efficiency permits a value of collection efficiency greater than 1 for infinitely large droplets when the airfoil is at an angle of attack other than zero. The total rate of water interception can also be found in terms of the collection efficiency given in figure 4 for the 65_1-212 airfoil from the relation

$$W_m = 0.329\ E_m\ TLUw \qquad (6)$$

where U is in miles per hour.

The value of the collection efficiency decreases with increasing values of the scale parameter ψ. At constant altitude, an increase in ψ is equivalent to an increase in the chord length with the same size droplets or equivalent to a decrease in the droplet size with the same airfoil chord length. The effect of wing taper can easily be obtained from the results of figure 4. For an airfoil with a 12-foot chord at the root section and a 3-foot chord at the tip section, the scale parameter ψ changes from 1675 at the root to 419 at the tip when the airfoil is moving at 400 miles per hour at an altitude of 30,000 feet through a cloud composed of droplets 17 microns in diameter ($Re_0 = 90$). The collection efficiency increases from 0.19 at the root to 0.42 at the tip of the airfoil. Although the collection efficiency at the root is 19/42 as large as that at the tip, the amount of water impinging on the root section is 1.8 times the amount impinging on the tip section because the root section is four times as large as the tip section (equation (6)).

The collection efficiency for the NACA 65_1-212 airfoil is compared in figure 5 with the collection efficiencies of a Joukowski airfoil and an NACA 65_2-015 airfoil, both of which are symmetrical and 15 percent thick, at an angle of attack of 4°. The collection efficiencies for the Joukowski and NACA 65_2-015 airfoils were obtained from reference 5. The 65_1-212 airfoil has a higher collection efficiency, in general, than the 15-percent-thick symmetrical airfoils, except for a portion of the curve at the lowest Reynolds number studied. The difference in collection efficiencies between the airfoils of two thicknesses becomes greater for the lower range of E_m and large values of ψ, which correspond to combinations of large values of chord length with small droplets. The higher collection efficiencies of the NACA 65_1-212 airfoil may be attributed to the fact that the 65_1-212 airfoil is thinner and has a sharper leading edge than the other two airfoils and also has a slight camber.

A comparison of the collection efficiency between the 65_1-212 airfoil and the two symmetrical airfoils is also tabulated in table I for several conditions of speed, altitude, chord length, and droplet size. With all three airfoils the effect on collection efficiency of a change in altitude from 10,000 to 30,000 feet is found to be small except for the conditions involving droplets larger than 40 microns in diameter. The effect of altitude can be found from table I by a comparison of alternating rows.

The effect of altitude on the amount of water impingement can also be studied from the results presented in figure 2. The values of $1/K = 21.8$ and $Re_0 = 325$ represent the conditions for an airfoil with a 12-foot chord traveling at 400 miles per hour through a cloud composed of droplets 17 microns in diameter at an altitude of 1000 feet. An increase in altitude from 1000 feet to 30,000 feet decreases the values of Re_0 to 92 and $1/K$ to 19.7 (speed, chord length, and droplet size are not changed). The value of $y_{0,u} - y_{0,l}$ changes from 0.021 to 0.023, or an increase of 9 percent. The effect of moderate changes in altitude may be ignored, because the droplet size and the liquid-water content of the cloud are seldom known with accuracy sufficient to permit the rate of water collection to be calculated within 10 percent accuracy.

The effect of a change in droplet size on the collection efficiency is exemplified by a comparison of row 9 with row 11 in table I. A change in droplet size from a diameter of 50 microns to a diameter of 5 microns reduces the collection efficiency for the NACA 65_1-212 airfoil from 0.68 to 0.10. For this example, the altitude was assumed to be 10,000 feet; the flight speed, 400 miles per hour; and the chord length, 3 feet.

Extent of impingement. - A knowledge of the extent of impingement is necessary for the design of anti-icing equipment. The extent of impingement is determined by the point of tangency on the airfoil of the tangent trajectories. The farthest points of impingement on the upper surface are shown in figure 6(a); and those on the lower surface, in figure 6(b). The extents of impingement for the 65_1-212 airfoil are also listed in table I for some flight and operating conditions. The distances S_u and S_l are measured on the surface from the point of intersection of the geometric chord line with the leading edge (fig. 1) in terms of the chord length.

The extent of impingement along the upper and lower surfaces is summarized in figure 7 for the same speeds, chord lengths, droplet sizes, and altitude as given in figure 3. The extent of impingement on both the upper and lower surfaces increases with increasing speed and with decreasing chord length. It is much greater along the lower surface than along the upper surface. As an example, for an airfoil with a 12-foot chord traveling at 400 miles per hour through a cloud composed of droplets 17 microns in diameter at an altitude of 10,000 feet ($Re_0 = 187$ and $\psi = 3590$), the ratio of the extent of impingement to the chord length on the upper surface is 0.013 and on the lower surface is 0.09 (fig. 6).

Cumulative collection efficiency. - The cumulative collection efficiency for any trajectory intermediate between the upper and the lower tangent trajectories (fig. 1) may be defined as

$$E = \frac{(y_0 - y_{0,l}) \cos \alpha}{T} \tag{7}$$

The droplet impingement between the lower tangent trajectory and any other trajectory is shown in figure 8 as a ratio to the maximum impingement. The ratio is

$$\frac{E}{E_m} = \frac{y_0 - y_{0,l}}{y_{0,u} - y_{0,l}} \tag{8}$$

The amount of water impinging on the airfoil between the farthest point of impingement on the lower surface and any other point of impingement on the surface may be found from the curves of figure 8 and the relation

$$W = 0.329 \left(\frac{E}{E_m}\right) E_m TLUw \cos \alpha \tag{9}$$

If a 12.5-foot-chord airfoil were traveling at 400 miles per hour at an altitude of 10,000 feet through a cloud composed of droplets 25 microns in diameter ($1/K = 10$, $Re_0 = 256$, $\psi = 2540$), the ratio of the farthest point of impingement to the chord length on the lower surface is 0.14 (fig. 8(b)). The amount of water impinging between the 0.14 point and any other point, such as the 0.04 point on the lower surface, is found by substituting into equation (9) the value of E/E_m for $S = -0.04$ and $1/K = 10$ obtained from figure 8(b) ($E/E_m = 0.24$). The value of E_m required in equation (9) is obtained from figure 4 ($E_m = 0.23$). For the airfoil in the preceding example, 24 percent of the total water W_m impinges between the 0.14 and the 0.04 points on the lower surface. For the same example, 84 percent of the total water W_m impinges on the lower surface of the airfoil and 16 percent, on the upper surface. In the limiting case of infinitely large droplets ($1/K = 0$), 65 percent of the total water impinges on the lower surface.

The effect of varying free-stream Reynolds number on the cumulative collection efficiency can be determined from figure 9. Figure 9 is also presented as an aid in the interpolation of results intermediate to the free-stream Reynolds numbers given.

Local rate of droplet impingement. - In the design of thermal anti-icing systems based on the principle of maintaining the water in the liquid state or on the principle of complete evaporation of the impinging water, a knowledge of the local rates of water impingement is required. The local rate of droplet impingement per unit area of airfoil surface can be determined from the expression

$$W_\beta = 0.329\ Uw \frac{dy_0}{dS} \cos \alpha = 0.329\ Uw\ \beta \cos \alpha \tag{10}$$

The values of β as a function of the airfoil distance S are given in figure 10. These values were obtained from the slopes of the curves in figure 8 by the relation

$$\beta = \frac{\Delta(E/E_m)}{\Delta S} (y_{0,u} - y_{0,l}) \tag{11}$$

In cyclical thermal de-icing systems a spanwise parting strip is usually located near the air stagnation line, which is located at $S_l = 0.008$ for the airfoil considered herein. The maximum rate of local impingement coincides very nearly with the proper location of the parting strip (fig. 10).

The data presented in figures 2 to 10 apply directly to flights in clouds composed of droplets that are all uniform in size. The water droplets in a cloud, however, are not necessarily uniform in size; the extent of impingement is always determined by the largest droplets in the cloud. The local rates of impingement are determined by the droplet-size distribution patterns present in the cloud. For flights in clouds composed of droplets that are not uniform in size, the β curves of figure 10 must be altered to conform with the weighted basis of the droplet-size distribution.

CONCLUDING REMARKS

Water-droplet trajectory data for an NACA 65_1-212 airfoil at an angle of attack of 4° were calculated, and the collection efficiencies, impingement areas, and rates of impingement were evolved from the calculations. A graphical procedure is presented to aid in the interpretation of airplane speed, chord length, altitude, and droplet diameter in terms of the dimensionless parameters used in the trajectory calculations. The relatively simple methods of solution will afford engineering data that were heretofore unavailable for the design of systems used in the protection of airfoils against ice formations.

Lewis Flight Propulsion Laboratory
National Advisory Committee for Aeronautics
Cleveland, Ohio

APPENDIX A

SYMBOLS

The following symbols are used in this report:

a	droplet radius, ft
C_D	drag coefficient for droplets
C_p	pressure coefficient
d	droplet diameter, microns (3.28×10^{-6} ft)
E	collection efficiency, based on maximum thickness of airfoil
K	inertia parameter, $\frac{2}{9} \frac{\rho_w a^2 U}{\mu L}$, where U is in ft/sec, dimensionless
L	airfoil chord length, ft
M	free-stream Mach number
p	absolute pressure, in. Hg
Re	Reynolds number with respect to droplet, $2a \rho_a \bar{v}/\mu$
r	distance from an element of the vortex sheet to a point in the flow field, ratio to chord length
S	distance from chord line measured on surface of airfoil, ratio to chord length
T	maximum airfoil thickness, ratio to chord length
T_a	most probable icing temperature (fig. 14), $^\circ R$
t	time, sec
U	flight speed or free-stream velocity, mph or ft/sec as noted
u	local air velocity, ratio to free-stream velocity
v	local droplet velocity, ratio to free-stream velocity
$\bar{v}$	local vector difference between velocity of droplet and velocity of air, ft/sec

W rate of water impingement, lb/(hr)(ft span)

W_β local rate of water impingement, lb/(hr)(sq ft)

w liquid-water content in cloud, g/cu m

x,y rectangular coordinates, ratio to chord length

α angle of attack, deg

β impingement factor, dimensionless

Γ vortex strength, dimensionless

γ ratio of specific heats, 1.4

μ viscosity, slugs/(ft)(sec)

ξ,η coordinate points on airfoil, ratio to chord length

ρ density, slugs/cu ft

τ time scale tU/L, where U is in ft/sec, dimensionless

ψ scale parameter, $\frac{9L}{a}\frac{\rho_a}{\rho_w} \equiv \frac{Re_0}{K}$, dimensionless

Subscripts:

0 free stream

a air

l lower airfoil surface

m maximum

s airfoil surface

u upper airfoil surface

v vortex

w water

x horizontal component

y vertical component

APPENDIX B

METHOD USED TO CALCULATE INCOMPRESSIBLE FLOW FIELD AROUND AIRFOIL

The velocity at the surface of an airfoil can be determined from a knowledge of the pressure coefficient C_p and the free-stream Mach number M with the aid of the following expression:

$$u_s = \sqrt{1 + \frac{2}{(\gamma-1)M^2}\left[1 - \left(\frac{C_p \gamma M^2 + 2}{2}\right)^{\frac{\gamma-1}{\gamma}}\right]} \qquad (B1)$$

The pressure coefficients for a large number of points on the surface of the NACA 65_1-212 airfoil at an angle of attack of 4° were obtained from wind-tunnel data taken at the Ames laboratory for several free-stream Mach numbers. The data are for a section of a wing having aspect ratio of 9. The surface velocities, which were used to calculate the flow field, were calculated for a Mach number of 0.2 for this report. The flow fields at other Mach numbers were not calculated because other exploratory work has shown that the effect of the compressibility of the air on the trajectories of the droplets was negligible.

The velocities in the two-dimensional flow field were calculated by distributing a sheet of vortices on the airfoil surface of such strength that the velocities on the surface caused by the vortices were the same as the velocities calculated with the use of equation (B1). The velocity at a point in a flow field caused by an element of the vortex sheet of strength $\Delta\Gamma$ placed a distance r from the point is

$$u_v = \frac{\Delta\Gamma}{2\pi r}$$

If an element of vortex sheet of strength

$$\Delta\Gamma_i \equiv (u_s \Delta S)_i$$

is placed on an increment ΔS of the airfoil at the i^{th} position on the airfoil surface, the velocity caused only by the i^{th} section of the airfoil is

$$u_v = \frac{(u_s \Delta S)_i}{2\pi r_i}$$

at a point in the flow field at a distance r_i from the i^{th} section (fig. 11). The local components of the perturbation velocity, at a point in the flow field, caused by 300 vortex elements distributed on both the upper and the lower surfaces of the airfoil are

$$\left.\begin{aligned} u_{x,v} &= \sum_{i=0}^{300} \frac{u_s}{2\pi} \frac{y-\eta}{r^2} \Delta S \\ u_{y,v} &= \sum_{i=0}^{300} \frac{u_s}{2\pi} \frac{\xi-x}{r^2} \Delta S \end{aligned}\right\} \quad \text{(B2)}$$

The horizontal and vertical components of the local velocity u_x and u_y, respectively, are obtained by adding $\cos \alpha$ to $u_{x,v}$ and $\sin \alpha$ to $u_{y,v}$.

A total of 300 vortex elements were used on the airfoil with a much denser distribution on the forward section than beyond the 50-percent point. Equations (B2) were solved with the use of electronic calculating machines. Approximately 300 points were computed in the flow field out to 1 chord length ahead of the airfoil in the region of interest with regard to computing the trajectories of droplets that strike the airfoil. Between 1 chord length and 5 chord lengths ahead of the airfoil leading edge, the flow-field velocity components were approximated by assuming that the flow was caused by a single vortex located on the airfoil chord line 25 percent inward from the leading edge.

APPENDIX C

GRAPHICAL PROCEDURE FOR INTERPRETATION OF PRACTICAL FLIGHT CONDITIONS IN TERMS OF DIMENSIONLESS PARAMETERS

A graphical procedure is presented to aid in the interpretation of airplane speed, chord size, altitude, and droplet diameter into terms of the dimensionless parameters K, ψ, and Re_0 used in this report. A solution of equation (2) is presented in figure 12 for two altitudes. For given droplet diameters in microns and ratios of the chord length in feet to the flight speed in miles per hour, the reciprocal of the inertia parameter can be determined at altitudes of either 10,000 or 30,000 feet from figure 12. Altitude does not appreciably affect the value of $1/K$, as can be noted from either table I or a comparison of values in figure 12(a) with those in figure 12(b).

An airfoil with a 12-foot chord length at a flight speed of 400 miles per hour at an altitude of 30,000 feet passing through a cloud composed of droplets all of which are 17 microns in diameter will be used as an example in the graphical procedure to interpret practical flight units into terms of the dimensionless parameters. The value of $1/K$ is obtained from figure 12(b) for the values of $\frac{L}{U} = \frac{12}{400} = 0.0300$ and droplet diameter of $d = 17$. The value of $1/K$ obtained from figure 12(b) is 19.4.

The free-stream Reynolds number for different altitudes may be obtained from figure 13. The product of the droplet diameter in microns and the flight speed in miles per hour must be known. The Reynolds number is a function of the air density, which depends on the pressure and the temperature at the altitudes considered. The pressure used to calculate the air density was taken from tables of NACA standard atmospheric pressure at various altitudes, but the temperature was based on the most probable icing temperature at various altitudes. The most probable icing temperature was obtained from approximately 300 icing observations (reference 7) and is presented in figure 14. For the example under consideration, the product of the droplet diameter and the flight speed is $(17)(400) = 6800$. The value of Re_0 as obtained from figure 13 is 89.

The scale parameter ψ for various values of $1/K$ and Re_0 may be obtained from figure 15. For the example considered, $\psi = 1732$.

The following relations are presented for use when the degree of accuracy required is not attainable with the graphical procedure. The

values for the viscosity μ should be obtained from figure 16; these values are based on the most probable icing temperature of figure 14.

$$K = 1.704 \times 10^{-12} \frac{d^2 U}{\mu L}$$

$$Re_0 = 4.813 \times 10^{-6} \frac{d \rho_a U}{\mu}$$

$$d = 7.662 \times 10^{5} \sqrt{\frac{K \mu L}{U}}$$

$$\psi = 2.826 \times 10^{6} \frac{\rho_a L}{d}$$

$$\rho_a = 0.0412 \frac{p}{T_a}$$

$$W_m = 0.329 \, E_m \, TLUw$$

where

d	droplet diameter, microns
E_m	collection efficiency (as given in fig. 4)
K	inertia parameter, dimensionless
L	airfoil chord length, ft
p	absolute pressure, in. Hg
Re_0	free-stream Reynolds number with respect to droplet, dimensionless
T	maximum airfoil thickness, ratio to chord length
T_a	most probable icing temperature (fig. 14), $^{\circ}R$
U	flight speed, mph
W_m	maximum rate of water impingement, lb/(hr)(ft span)
w	liquid-water content in cloud, g/cu m
μ	viscosity, slugs/(ft)(sec)

ρ_a air density, slugs/cu ft

ψ scale parameter, dimensionless

(The density of water was assumed to be 62.46 lb/cu ft and the acceleration due to gravity, 32.17 ft/sec^2.)

REFERENCES

1. Glauert, Muriel: A Method of Constructing the Paths of Raindrops of Different Diameters Moving in the Neighborhood of (1) a Circular Cylinder, (2) an Aerofoil, Placed in a Uniform Stream of Air; and a Determination of the Rate of Deposit of the Drops on the Surface and the Percentage of Drops Caught. R. & M. No. 2025, British A.R.C., 1940.

2. Langmuir, Irving, and Blodgett, Katherine B.: A Mathematical Investigation of Water Droplet Trajectories. Tech. Rep. No. 5418, Air Materiel Command, AAF, Feb. 19, 1946. (Contract No. W-33-038-ac-9151 with Gen. Elec. Co.)

3. Bergrun, Norman R.: A Method for Numerically Calculating the Area and Distribution of Water Impingement on the Leading Edge of an Airfoil in a Cloud. NACA TN 1397, 1947.

4. Guibert, A. G., Janssen, E., and Robbins, W. M.: Determination of Rate, Area, and Distribution of Impingement of Waterdrops on Various Airfoils from Trajectories Obtained on the Differential Analyzer. NACA RM 9A05, 1949.

5. Bergrun, Norman R.: An Empirical Method Permitting Rapid Determination of the Area, Rate, and Distribution of Water-Drop Impingement of an Airfoil of Arbitrary Section at Subsonic Speeds. NACA TN 2476, 1951.

6. von Mises, Richard: Theory of Flight. McGraw-Hill Book Co., Inc., 1st ed., 1945.

7. Hacker, Paul T., and Dorsch, Robert G.: A Summary of Meteorological Conditions Associated with Aircraft Icing and a Proposed Method of Selecting Design Criterions for Ice-Prevention Equipment. NACA TN 2569, 1951.

TABLE I - COMPARISON OF ICING ON THREE AIRFOILS AT SEVERAL FLIGHT AND OPERATING CONDITIONS

[Angle of attack, 4°]

Row	Altitude (ft)	Speed (mph)	Chord length L (ft)	Droplet diameter d (microns)	Reciprocal of inertia parameter 1/K	Free-stream Reynolds number Re_0	Scale parameter Ψ	65_1-212 airfoil		Collection efficiency E_m		
								Distance from chord line on lower surface S_l (ratio to chord length)	Distance from chord line on upper surface S_u (ratio to chord length)	Airfoil		
										65_1-212	65_2-015	Joukowski
1	10,000	150	18	100.0	2.50	376.0	940	0.203	0.051	0.41	0.34	0.35
2	30,000	150	18	100.0	2.25	199.0	449	.237	.061	.47	.40	.41
3	10,000	150	18	15.6	100.00	58.7	5872	.030	.010	.07	.05	.02
4	30,000	150	18	15.6	90.00	31.0	2799	.036	.013	.08	.06	.03
5	10,000	300	9	17.0	20.50	128.0	2624	.080	.016	.17	.12	.09
6	30,000	300	9	17.0	19.00	67.8	1288	.088	.024	.19	.15	.12
7	10,000	300	16	17.0	37.50	128.0	4799	.057	.014	.12	.08	.05
8	30,000	300	16	17.0	33.50	67.8	2271	.062	.017	.14	.09	.06
9	10,000	400	3	50.0	.60	502.0	301	.371	.153	.68	.62	.66
10	30,000	400	3	50.0	.55	266.0	146	.410	.180	.76	.70	.75
11	10,000	400	3	5.0	60.00	50.0	3000	.047	.014	.10	.08	.04
12	30,000	400	3	5.0	55.00	26.6	1462	.054	.016	.11	.08	.05
13	10,000	450	6	17.0	9.40	192.0	1805	.117	.024	.25	.16	.15
14	30,000	450	6	17.0	8.50	102.0	867	.142	.032	.28	.22	.21
15	10,000	450	3	17.0	4.80	192.0	922	.163	.034	.35	.27	.25
16	30,000	450	3	17.0	4.30	102.0	437	.202	.036	.36	.33	.34

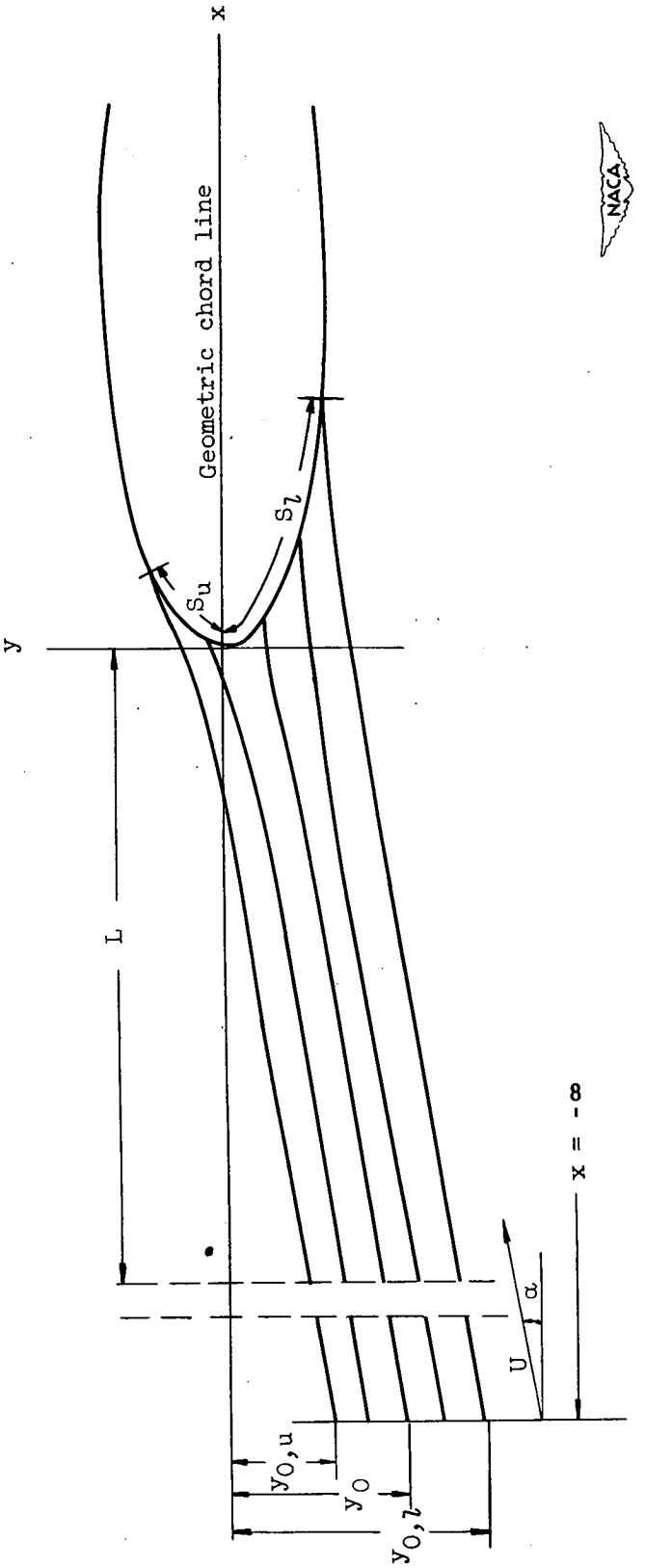

Figure 1. - Droplet trajectories with respect to airfoil.

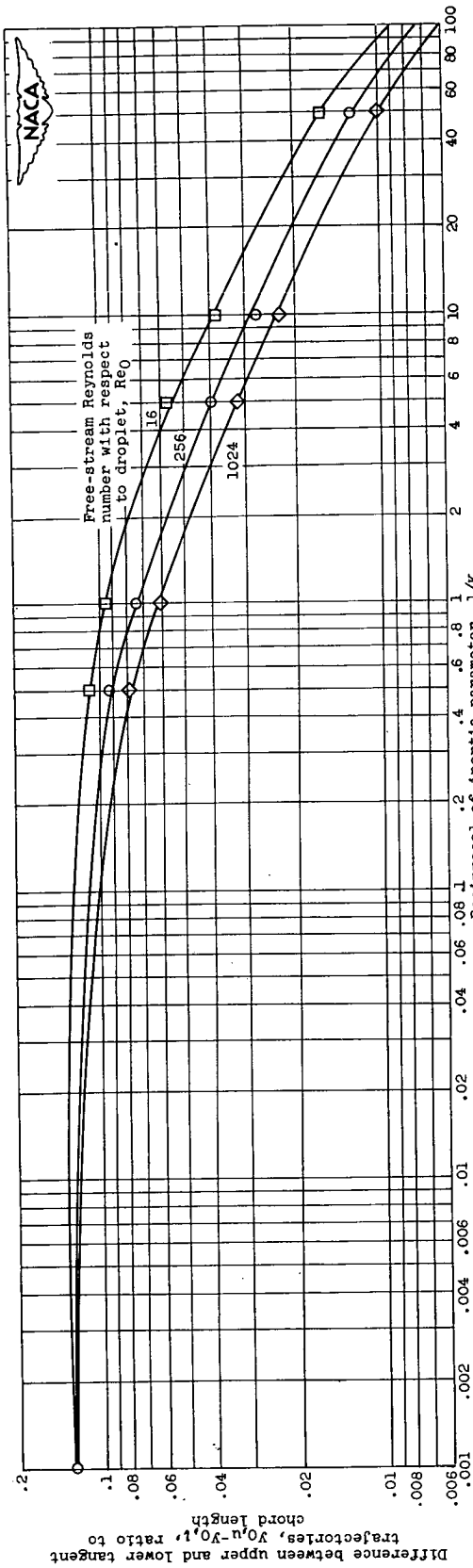

Figure 2. - Difference between upper and lower tangent trajectories at free-stream conditions. NACA 65_1-212 airfoil; angle of attack, 4°.

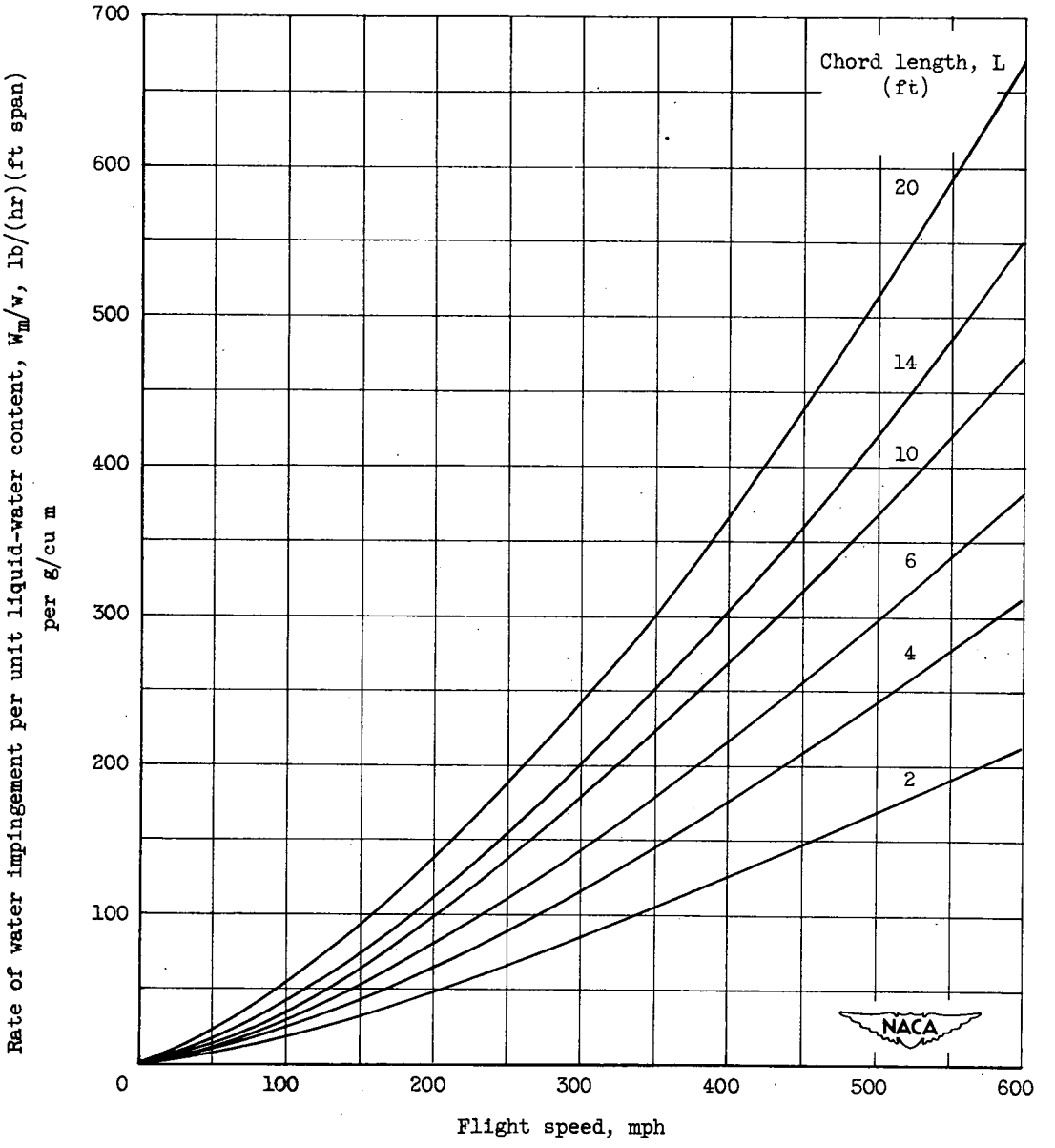

(a) Droplet size, 15 microns.

Figure 3. - Rate of water impingement. NACA 65_1-212 airfoil; angle of attack, 4°; altitude, 20,000 feet.

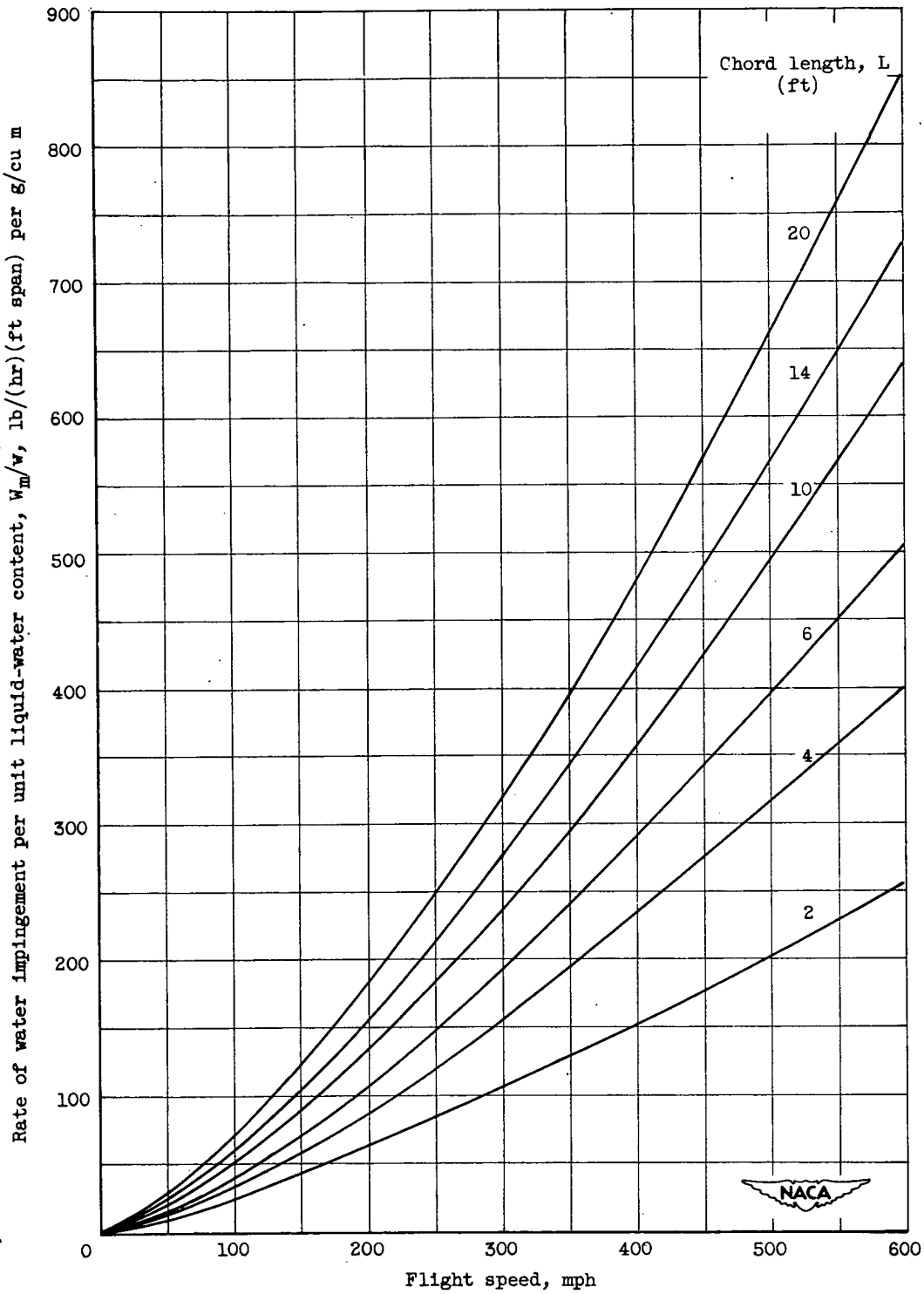

(b) Droplet size, 20 microns.

Figure 3. - Concluded. Rate of water impingement. NACA 65_1-212 airfoil; angle of attack, 4°; altitude, 20,000 feet.

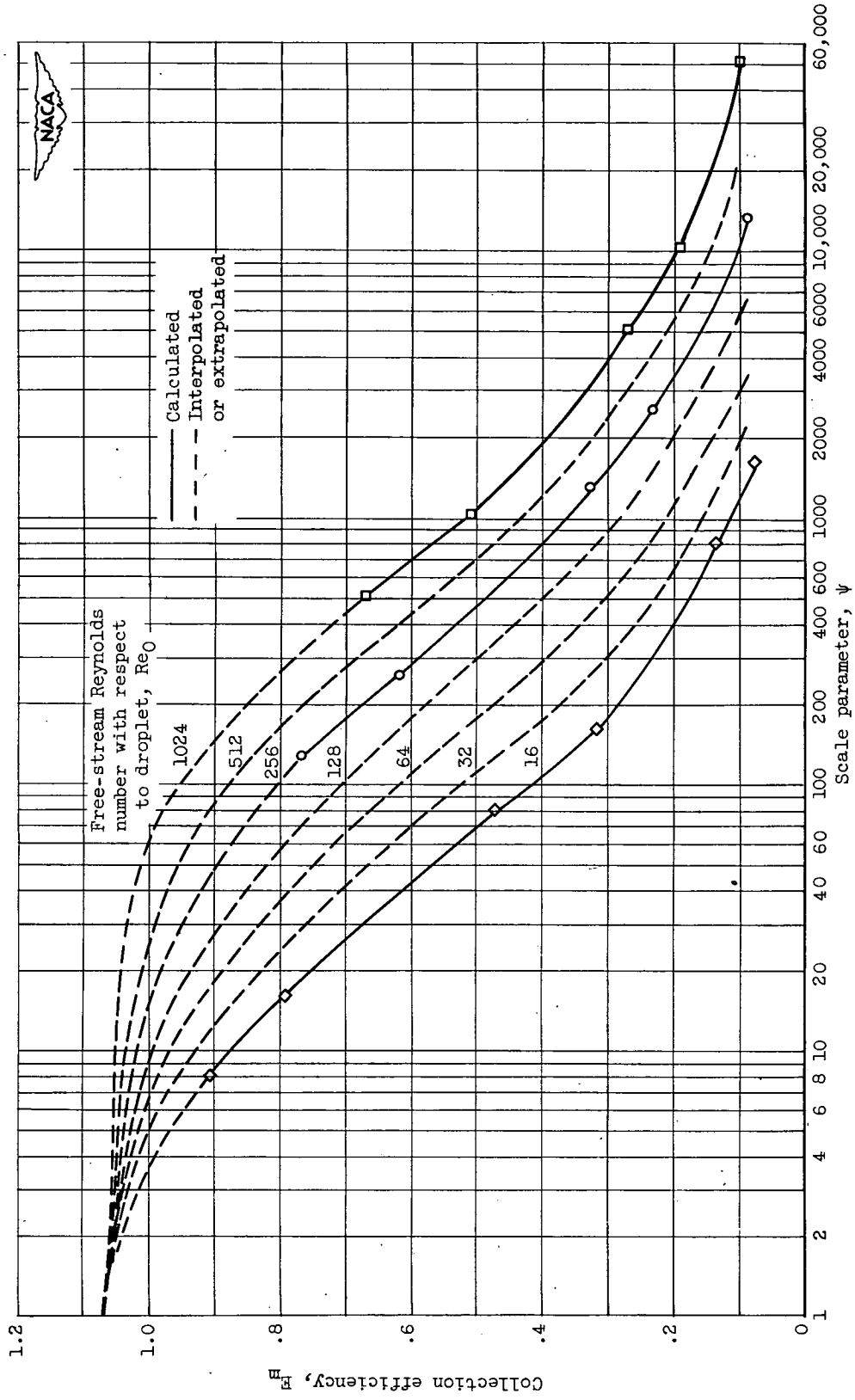

Figure 4. - Collection efficiency of NACA 65_1-212 airfoil as function of scale parameter. Angle of attack, 4°.

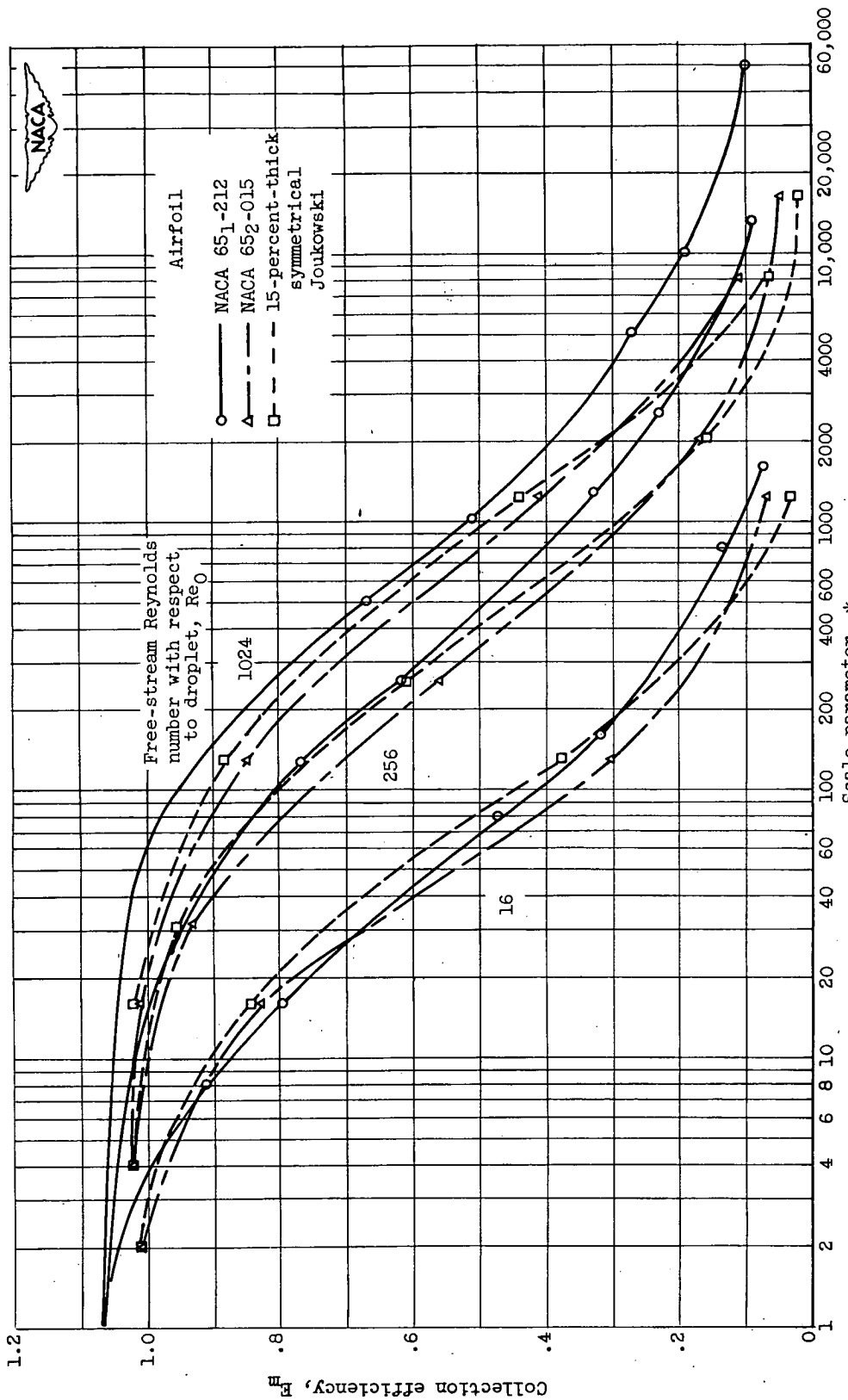

Figure 5. - Comparison of collection efficiency of NACA 65$_1$-212 airfoil with collection efficiencies of 15-percent-thick symmetrical Joukowski and NACA 65$_2$-015 airfoils. Angle of attack, 4°.

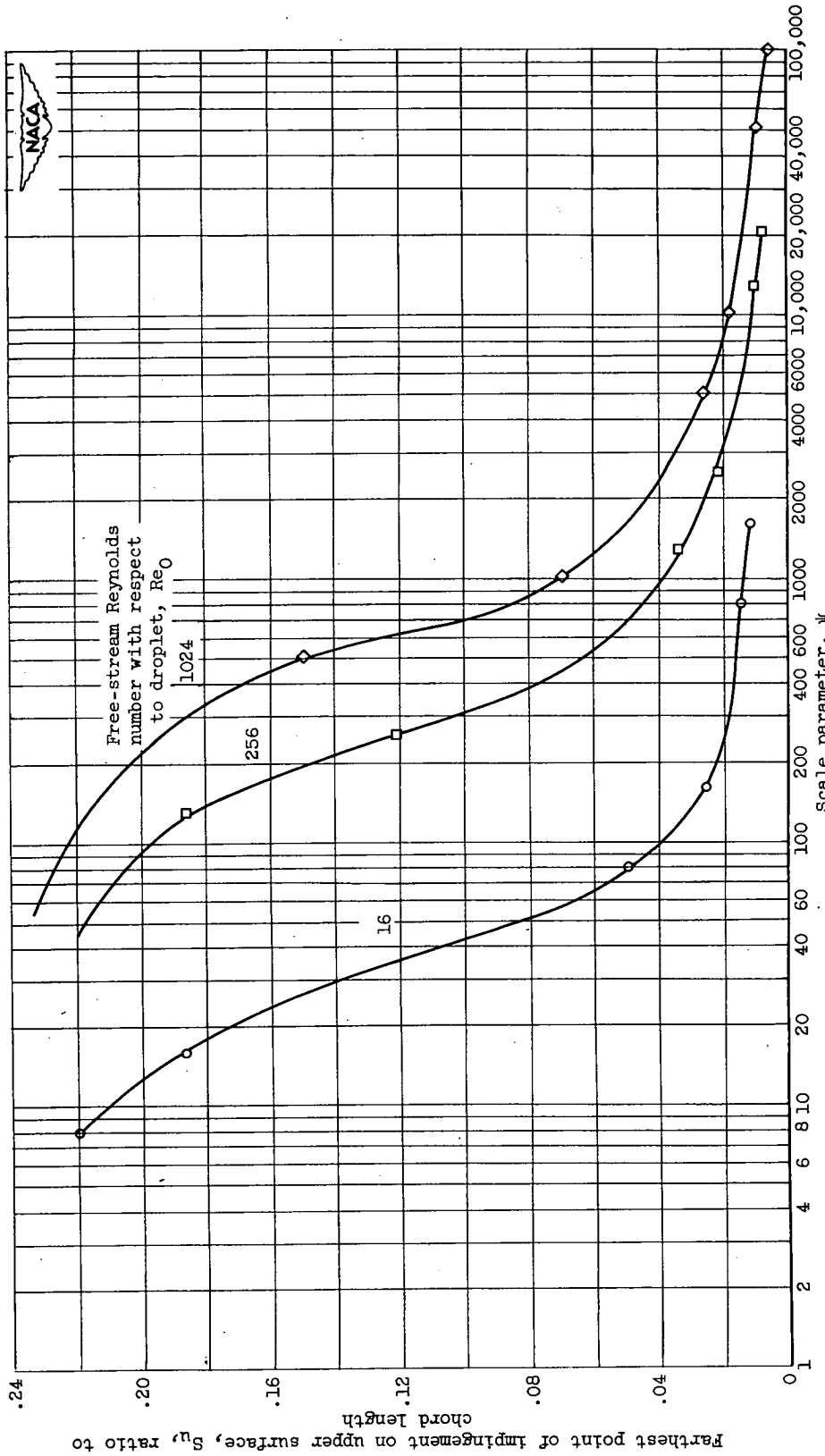

(a) Upper surface.

Figure 6. - Farthest point of droplet impingement on airfoil surface. NACA 65_1-212 airfoil; angle of attack, 4°.

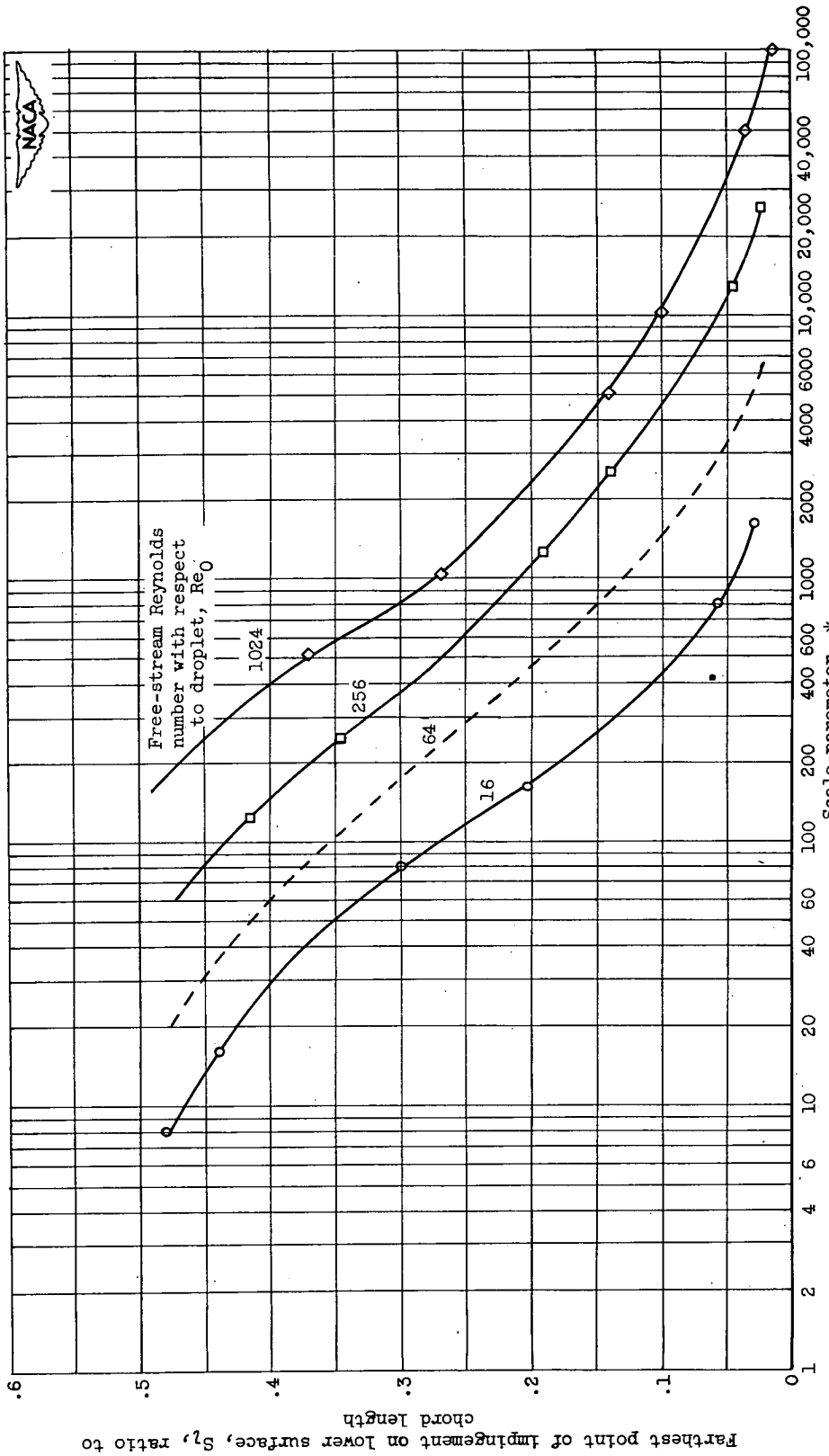

(b) Lower surface.

Figure 6. - Concluded. Farthest point of droplet impingement on airfoil surface. NACA 65_1-212 airfoil; angle of attack, 4°.

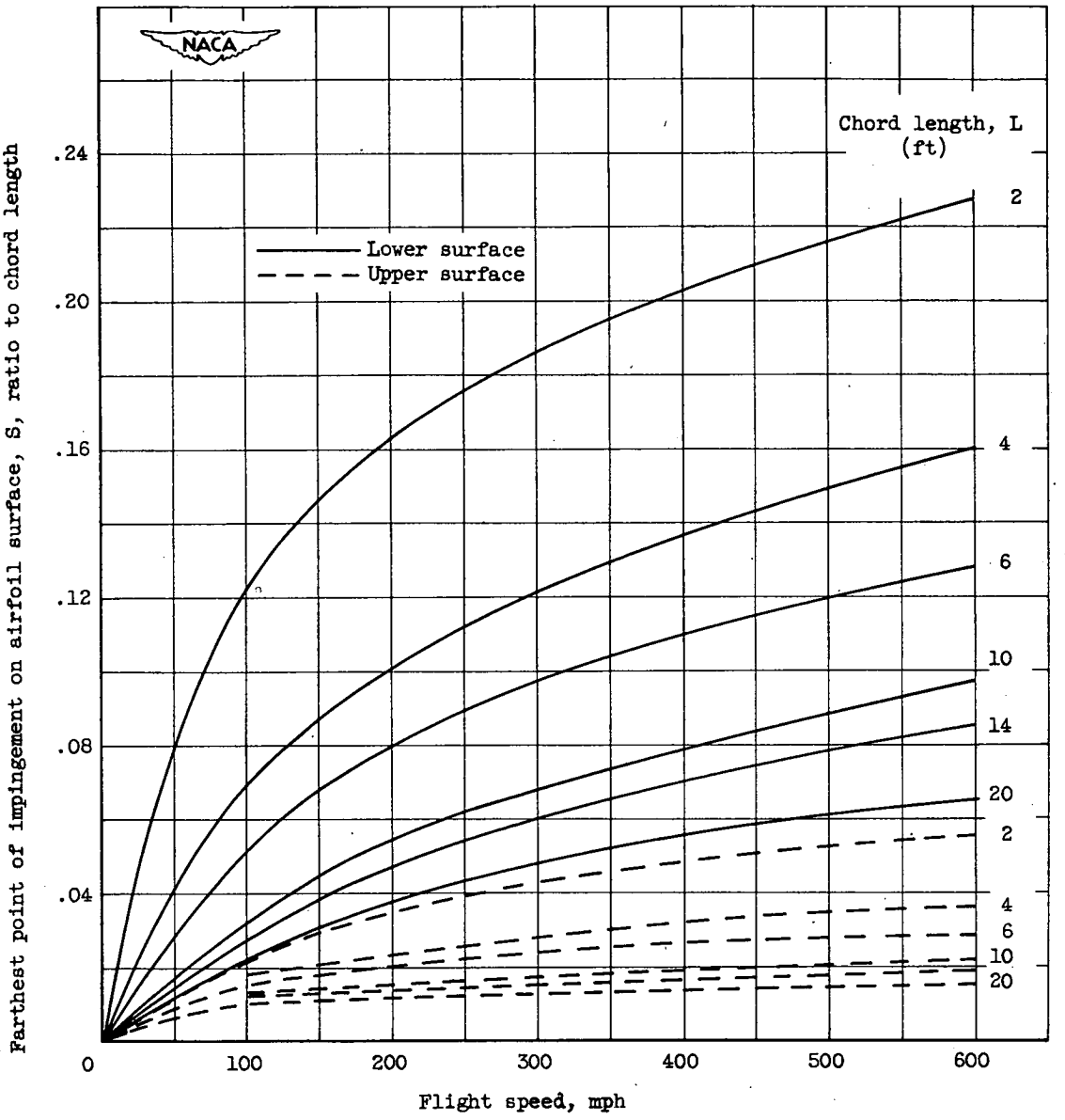

(a) Droplet size, 15 microns.

Figure 7. - Farthest point of impingement on airfoil surface as function of airspeed. NACA 65_1-212 airfoil; angle of attack, 4°; altitude, 20,000 feet.

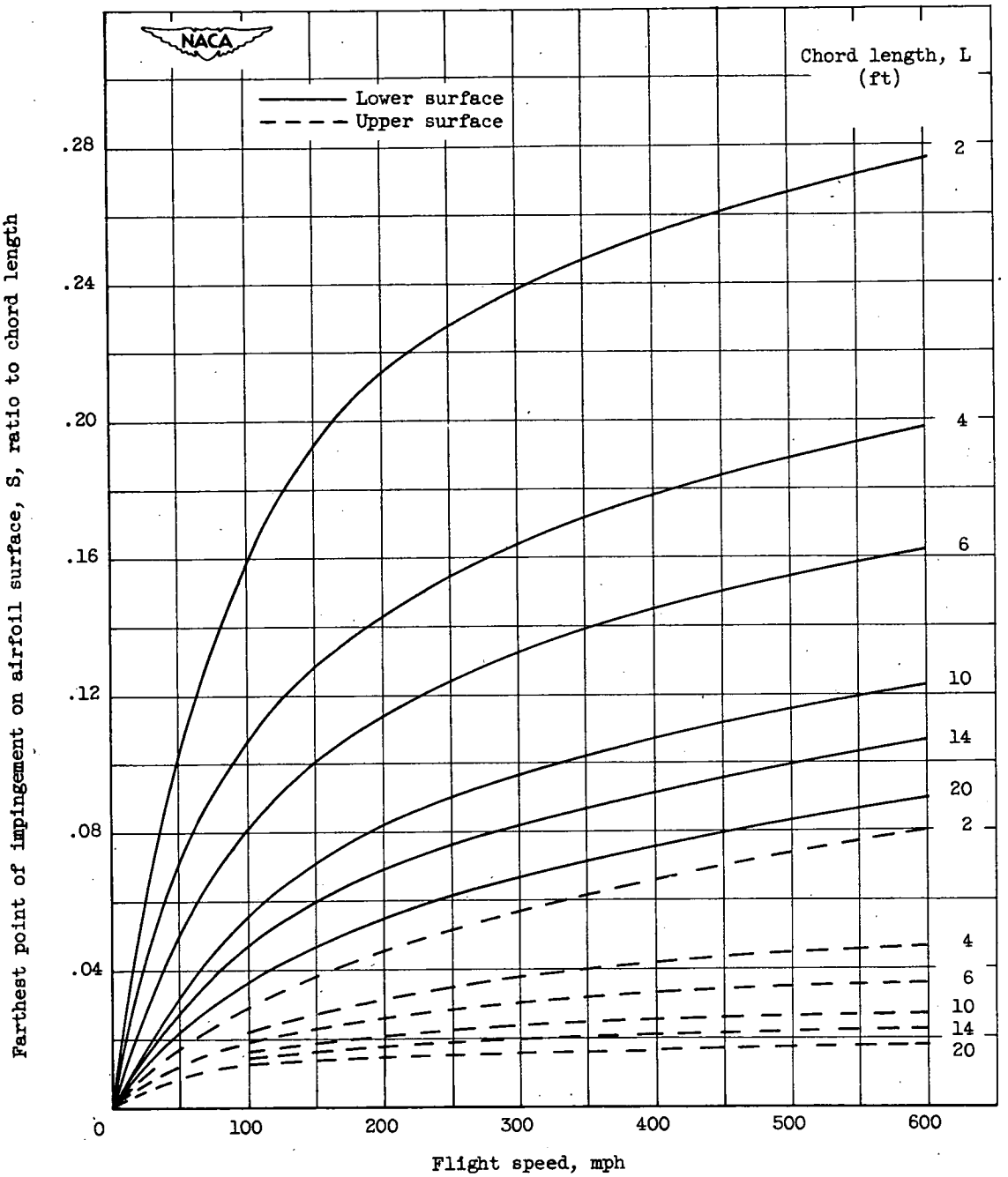

(b) Droplet size, 20 microns.

Figure 7. - Concluded. Farthest point of impingement on airfoil surface as function of airspeed. NACA 65_1-212 airfoil; angle of attack, 4°; altitude, 20,000 feet.

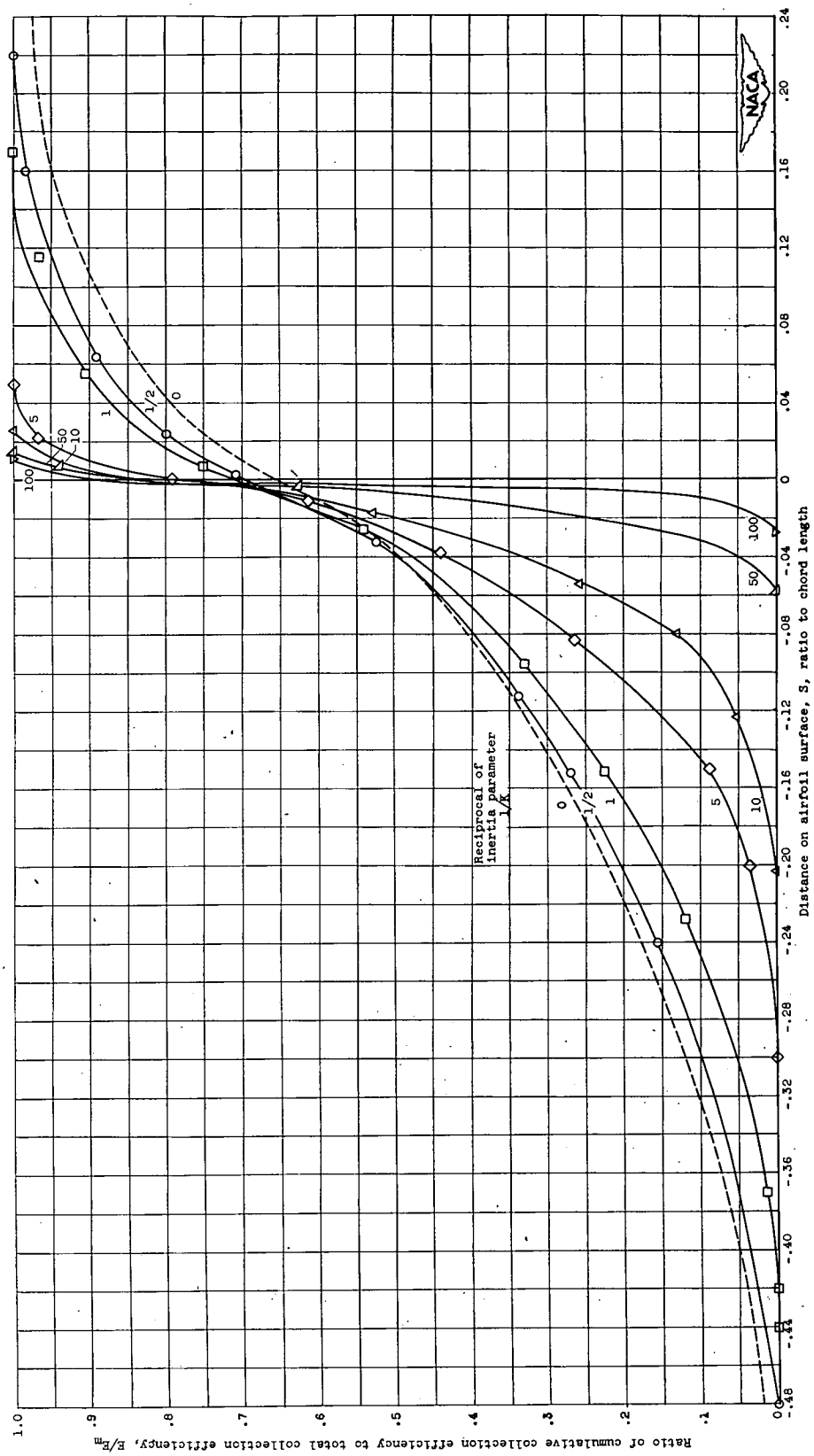

Figure 8. - Ratio of collection efficiencies as function of airfoil surface distance at constant free-stream Reynolds number with respect to droplet. NACA 65_1-212 airfoil; angle of attack, 4°.

(a) Free-stream Reynolds number with respect to droplet Re_0, 16.

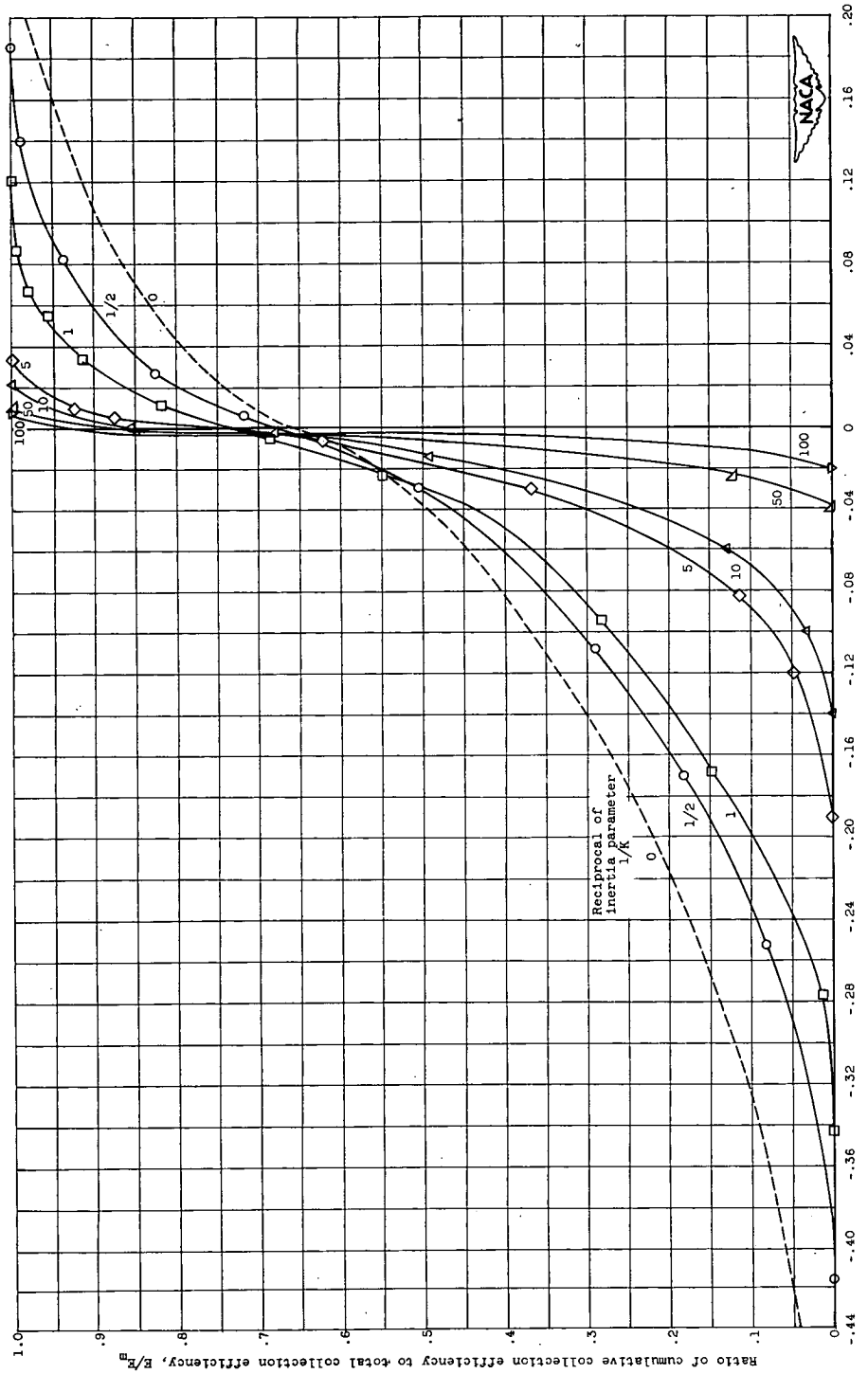

(b) Free-stream Reynolds number with respect to droplet Re_0, 256.

Figure 8. - Continued. Ratio of collection efficiencies as function of airfoil surface distance at constant free-stream Reynolds number with respect to droplet. NACA 65_1-212 airfoil; angle of attack, 4°.

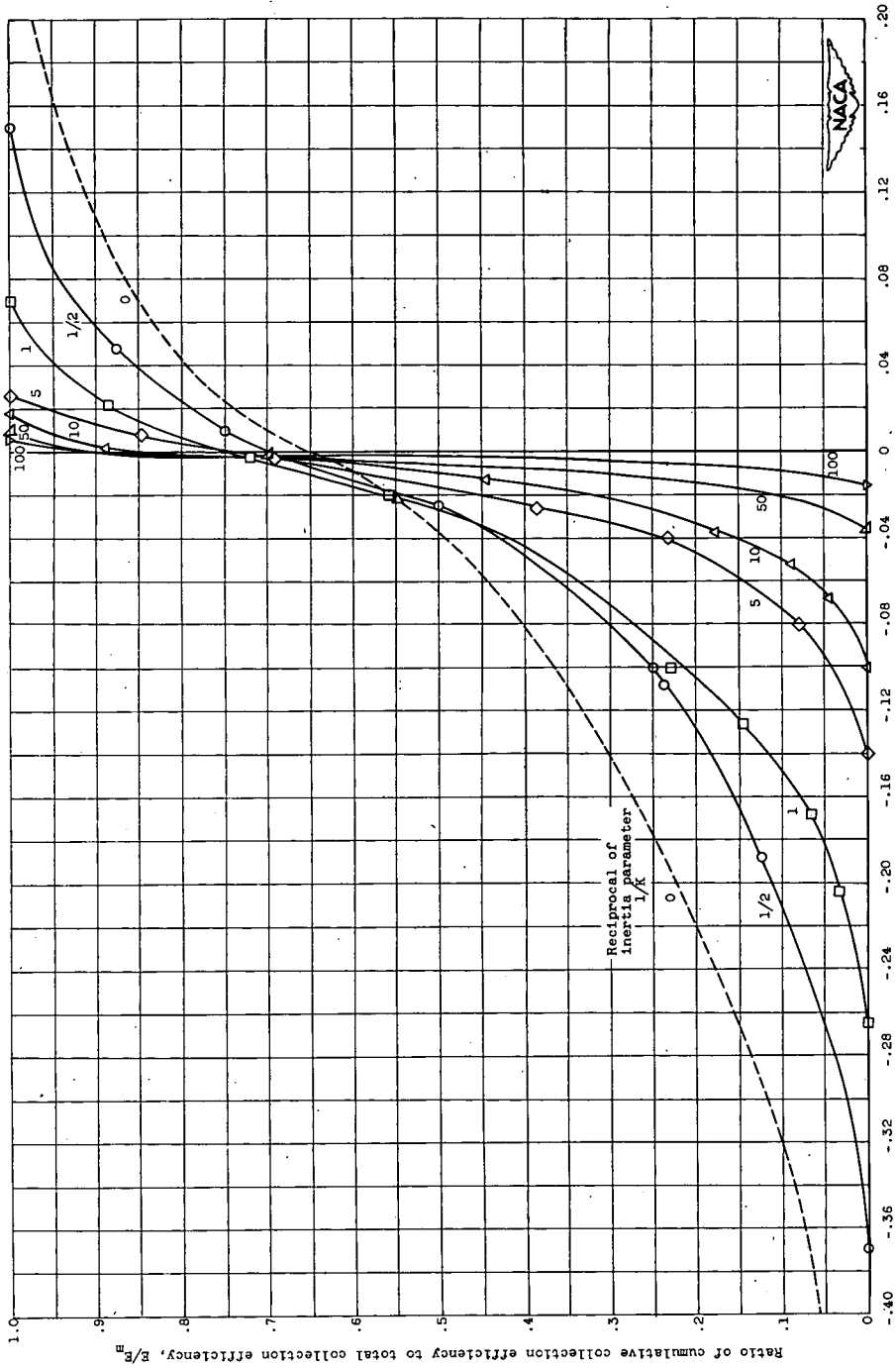

(c) Free-stream Reynolds number with respect to droplet Re_0, 1024.

Figure 8. - Concluded. Ratio of collection efficiencies as function of airfoil surface distance at constant free-stream Reynolds number with respect to droplet. NACA 65_1-212 airfoil; angle of attack, 4°.

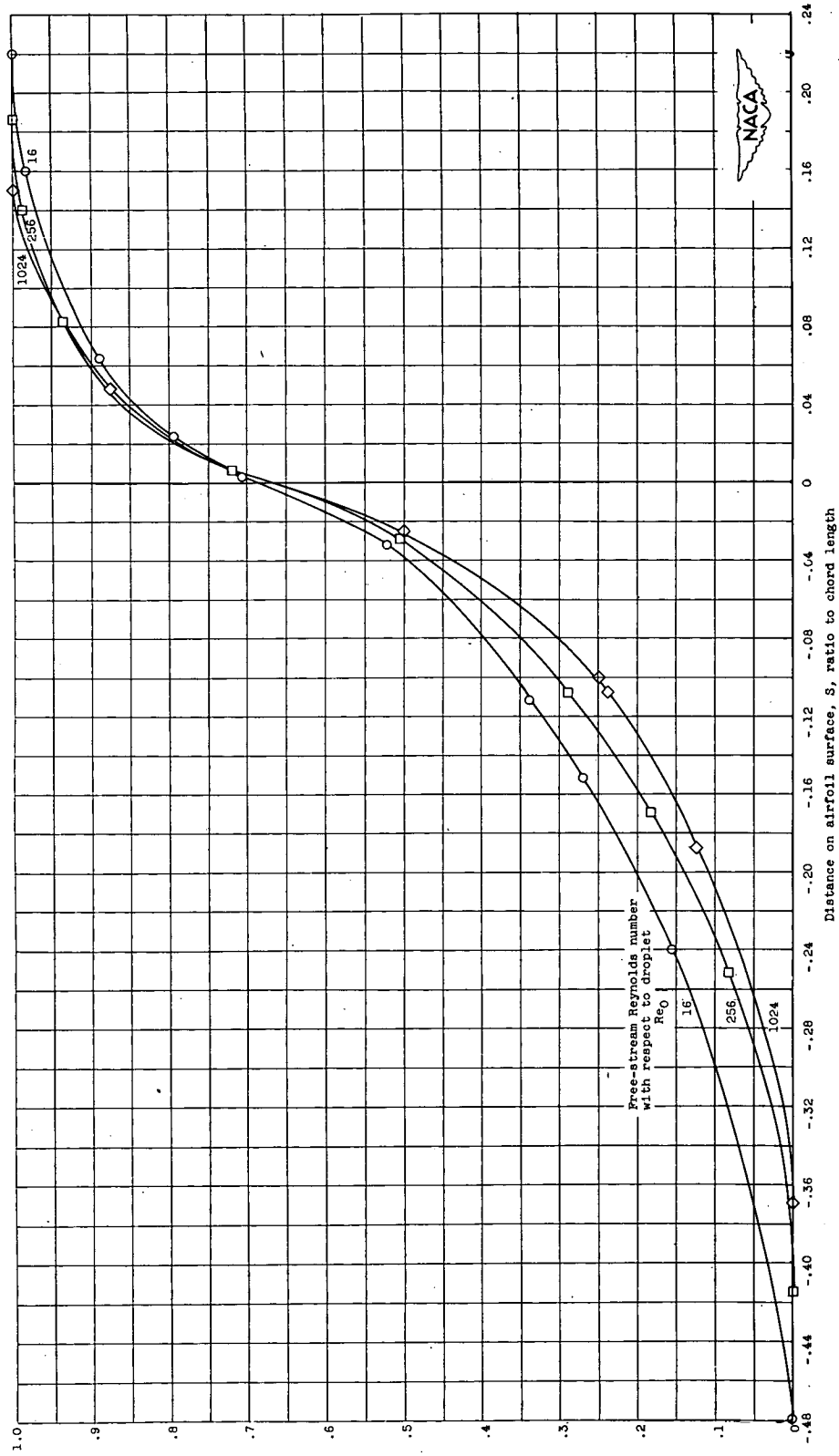

(a) Reciprocal of inertia parameter $1/K$, $1/2$.

Figure 9. - Ratio of collection efficiencies as function of airfoil surface distance at constant reciprocal of inertia parameter. NACA 65_1-212 airfoil; angle of attack 4°.

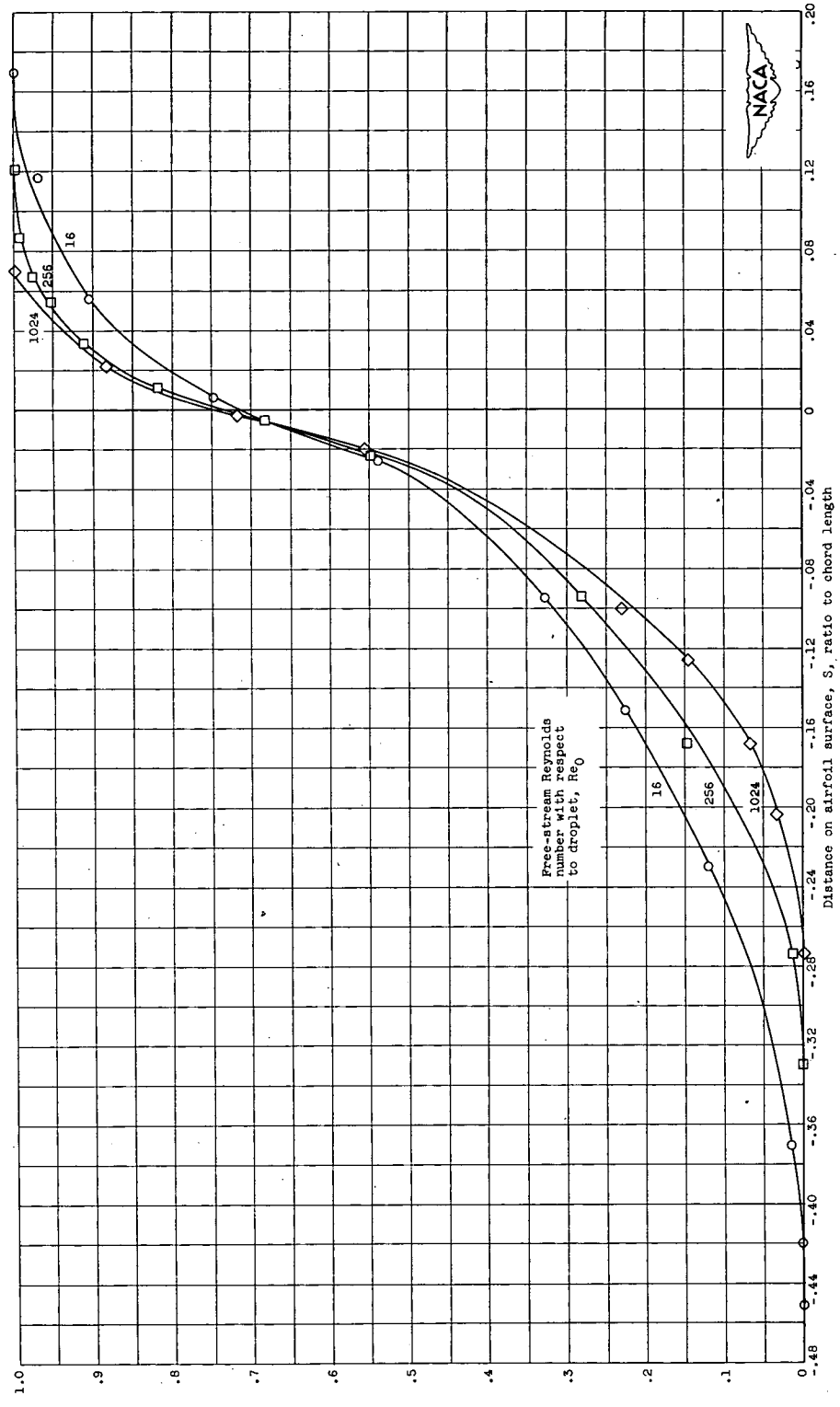

Figure 9. - Continued. Ratio of collection efficiencies as function of airfoil surface distance at constant reciprocal of inertia parameter. NACA 65_1-212 airfoil; angle of attack, 4°.

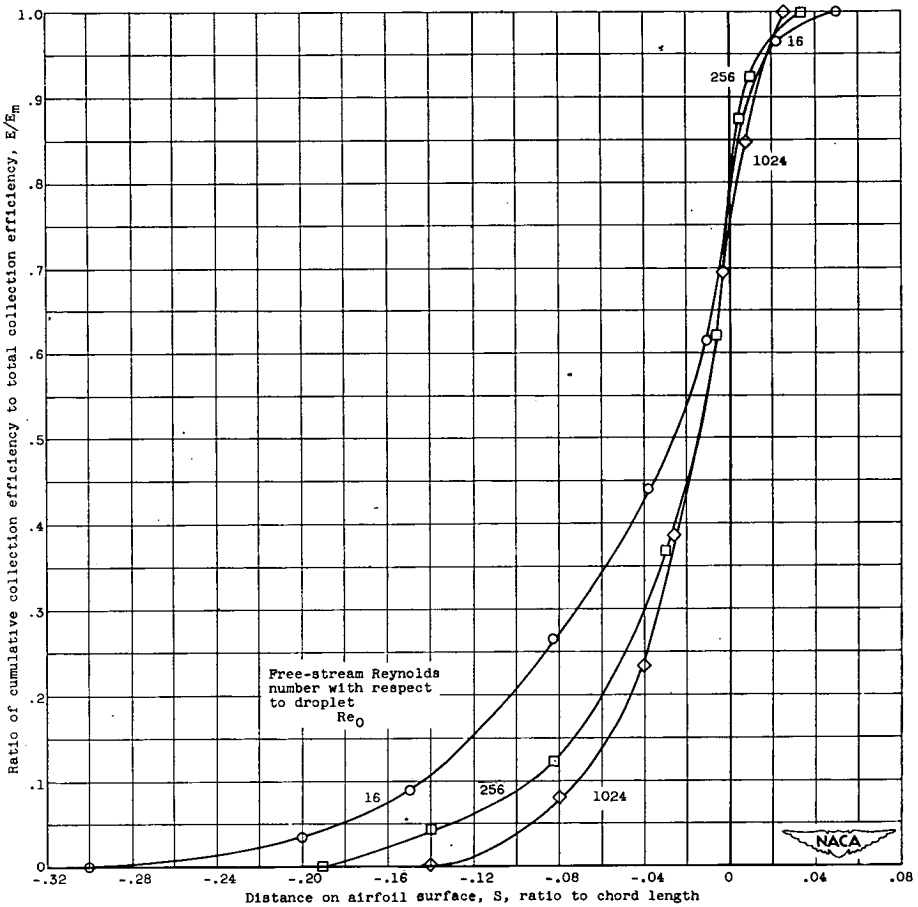

(c) Reciprocal of inertia parameter 1/K, 5.

Figure 9. - Continued. Ratio of collection efficiencies as function of airfoil surface distance at constant reciprocal of inertia parameter. NACA 65_1-212 airfoil; angle of attack, 4°.

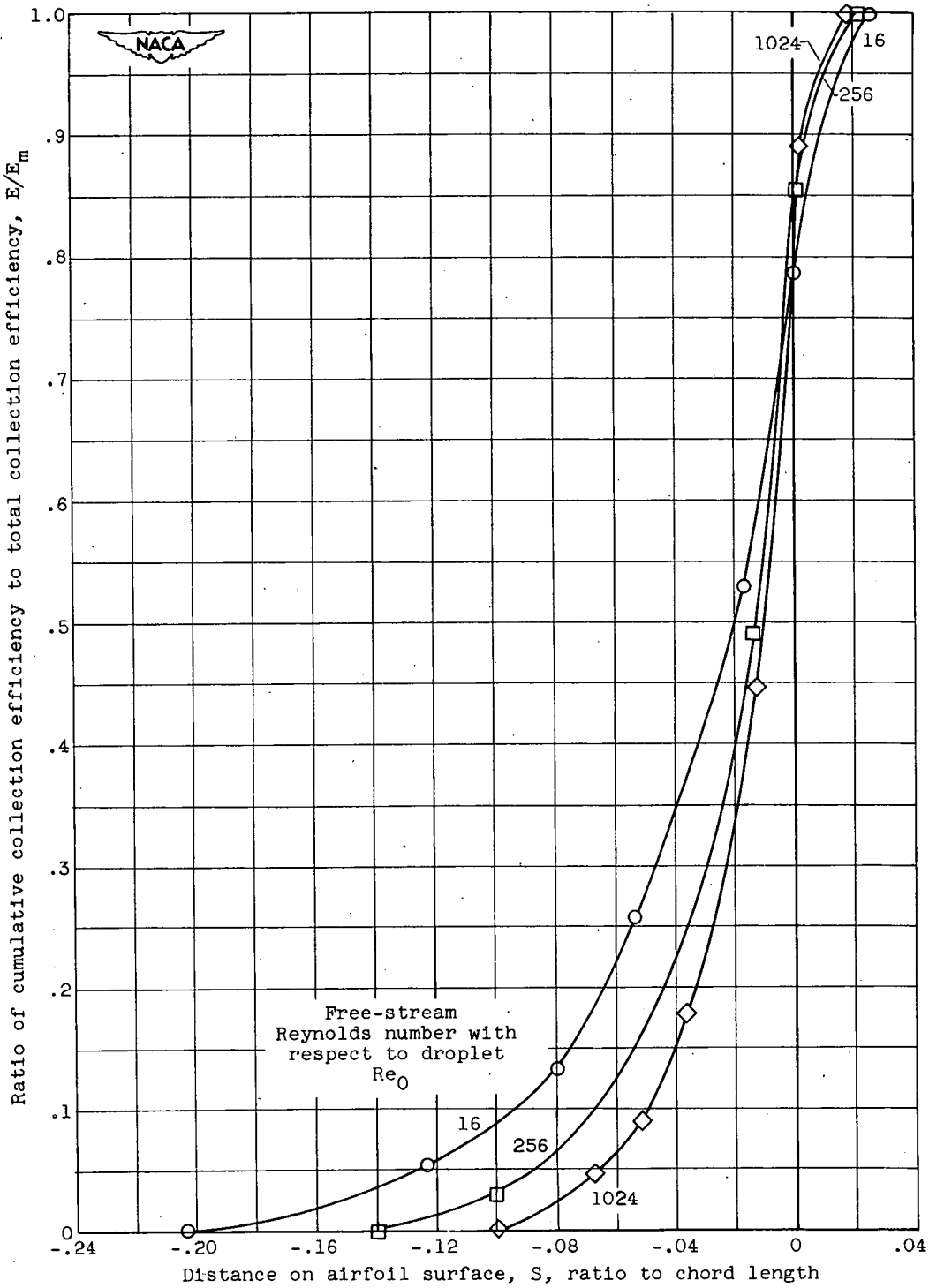

(d) Reciprocal of inertia parameter 1/K, 10.

Figure 9. - Continued. Ratio of collection efficiencies as function of airfoil surface distance at constant reciprocal of inertia parameter. NACA 65_1-212 airfoil; angle of attack, 4°.

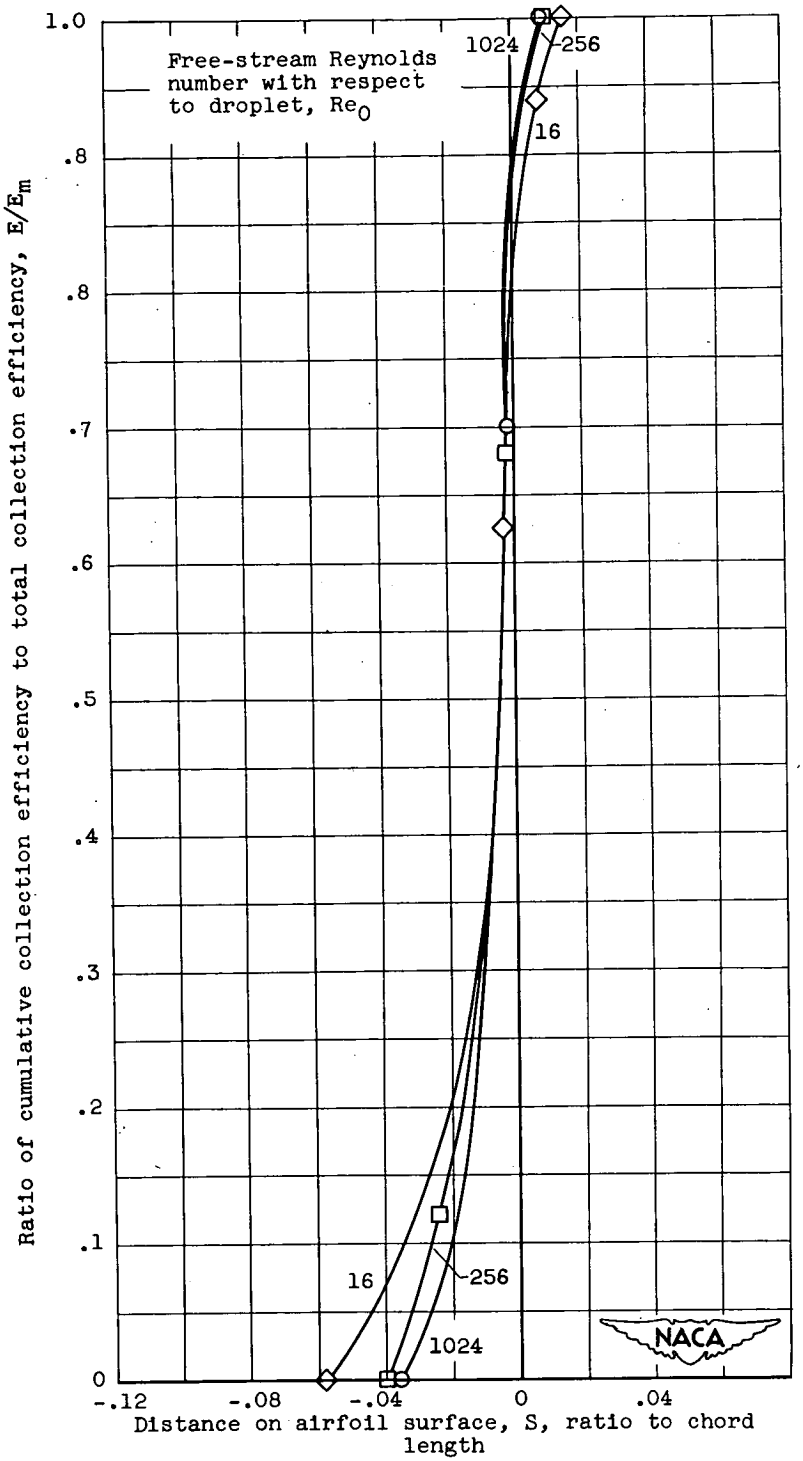

(e) Reciprocal of inertia parameter 1/K, 50.

Figure 9. - Concluded. Ratio of collection efficiencies as function of airfoil surface distance at constant reciprocal of inertia parameter. NACA 65_1-212 airfoil; angle of attack, 4°.

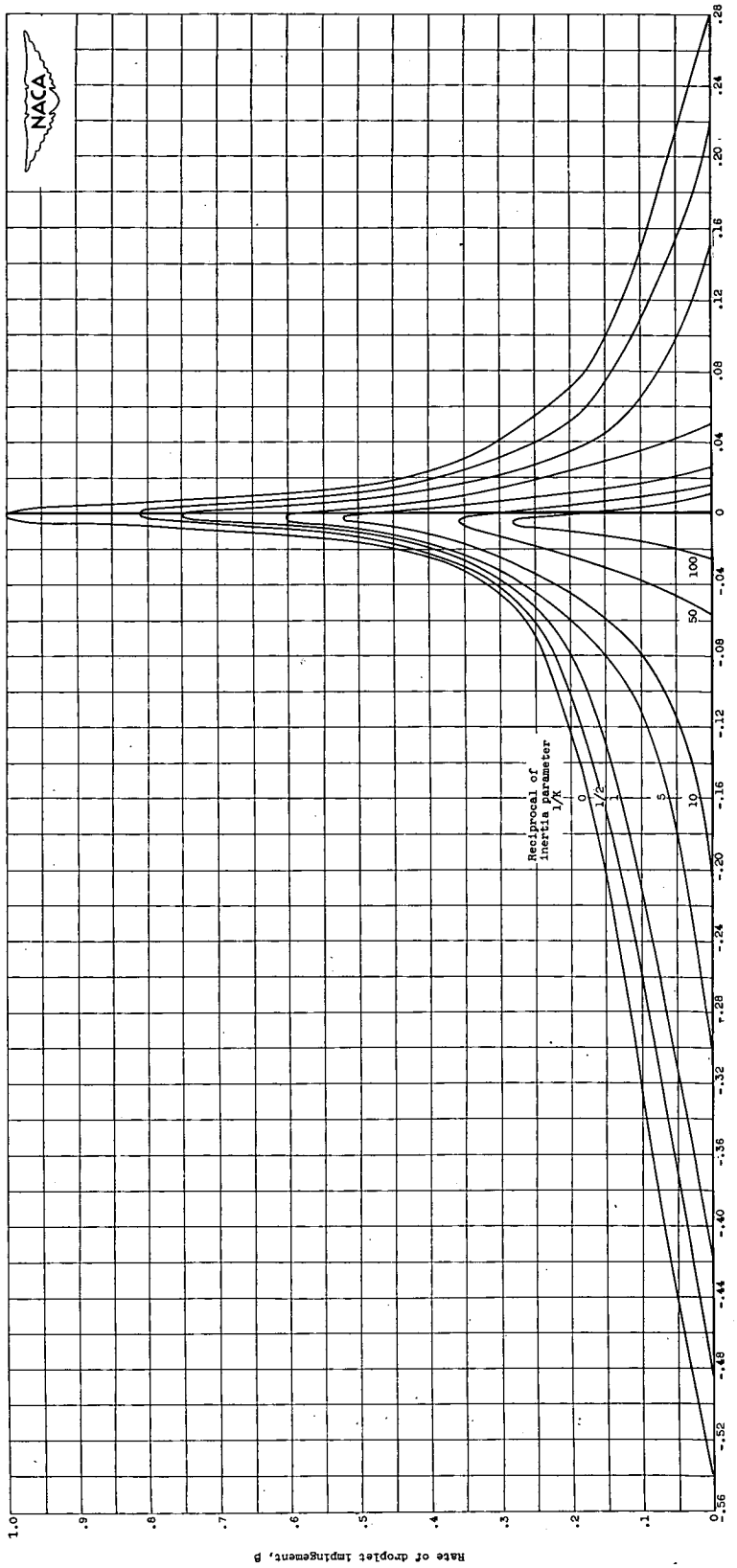

(a) Free-stream Reynolds number with respect to droplet, 16.

Figure 10. - Local rate of impingement, NACA 651-212 airfoil; angle of attack, 4°.

$$\beta = \frac{\Delta(E/E_m)}{\Delta S} \left(\gamma_{0,u} - \gamma_{0,l}\right)$$

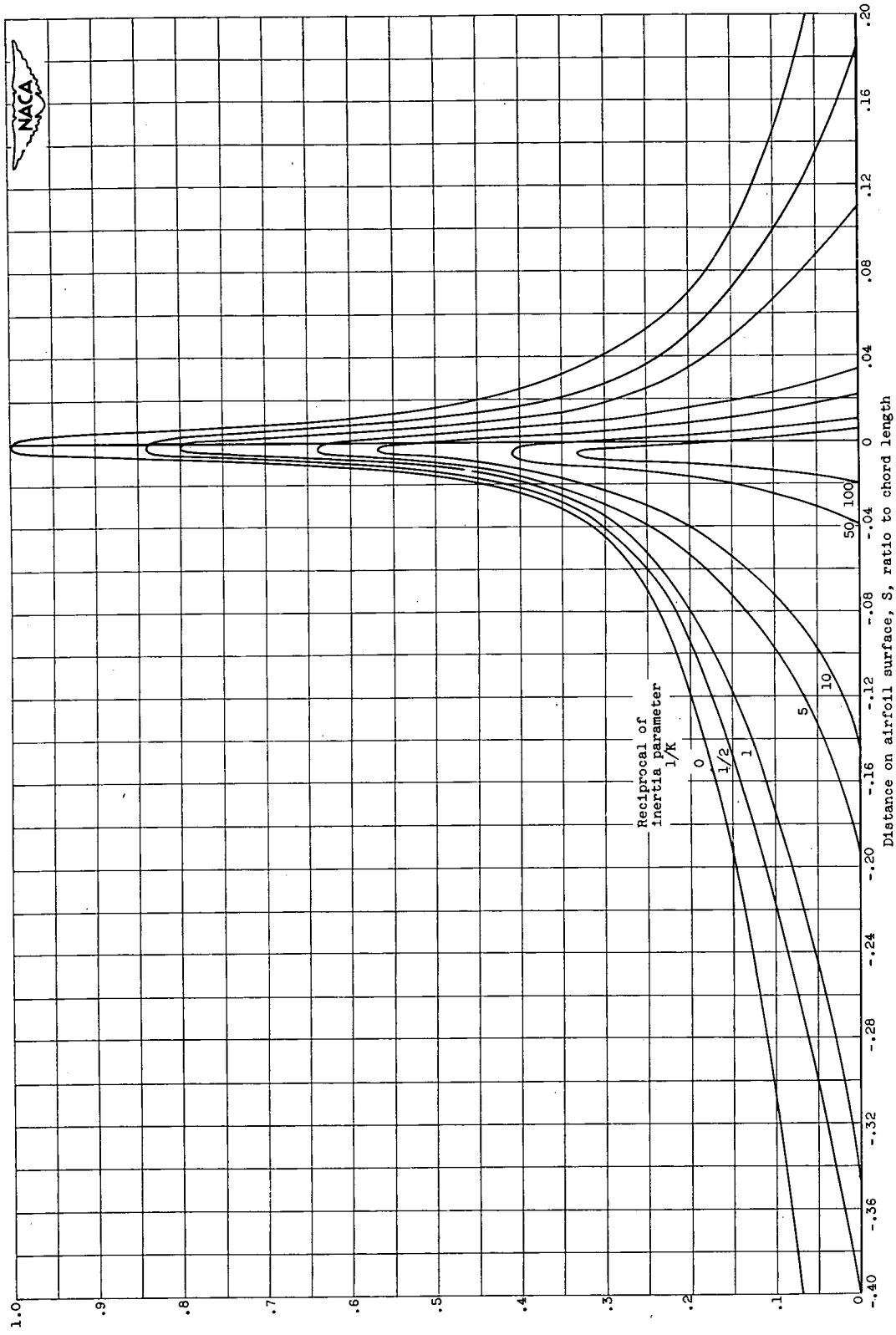

(b) Free-stream Reynolds number with respect to droplet, 256.

Figure 10. - Continued. Local rate of impingement. NACA 65$_1$-212 airfoil; angle of attack, 4°.

$$\beta = \frac{\Delta(E/E_m)}{\Delta S}\,(y_{O,u}-y_{O,l})$$

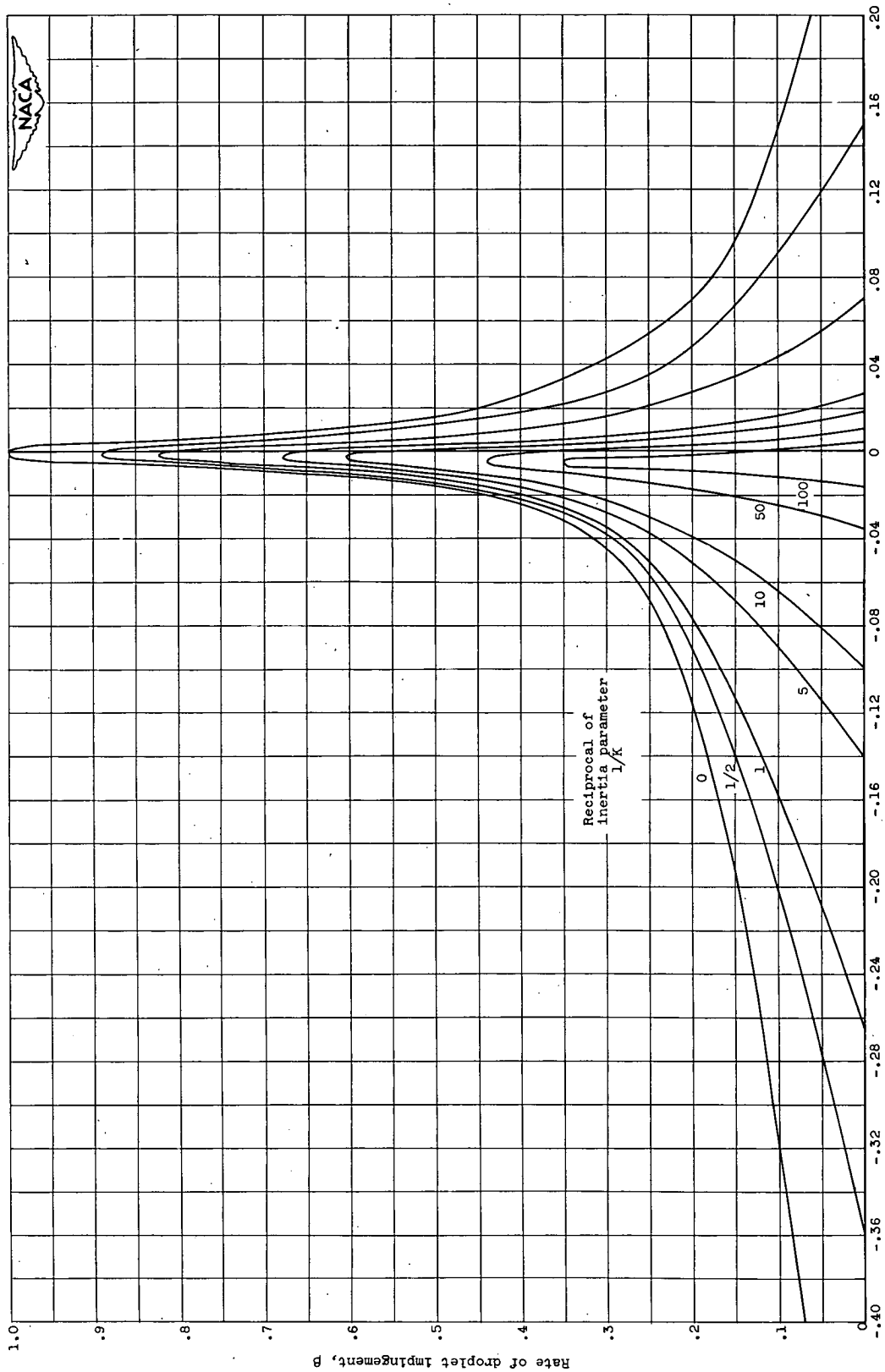

(c) Free-stream Reynolds number with respect to droplet, 1024.

Figure 10. - Concluded. Local rate of impingement. NACA 65_1-212 airfoil; angle of attack, 4°.

$$\beta = \frac{\Delta(E/E_m)}{\Delta S}\,(y_{0,u}-y_{0,l})$$

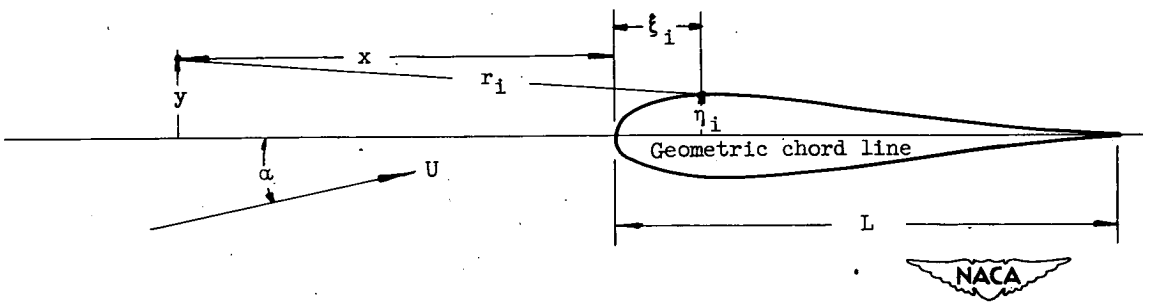

Figure 11. - Coordinate system for airfoil.

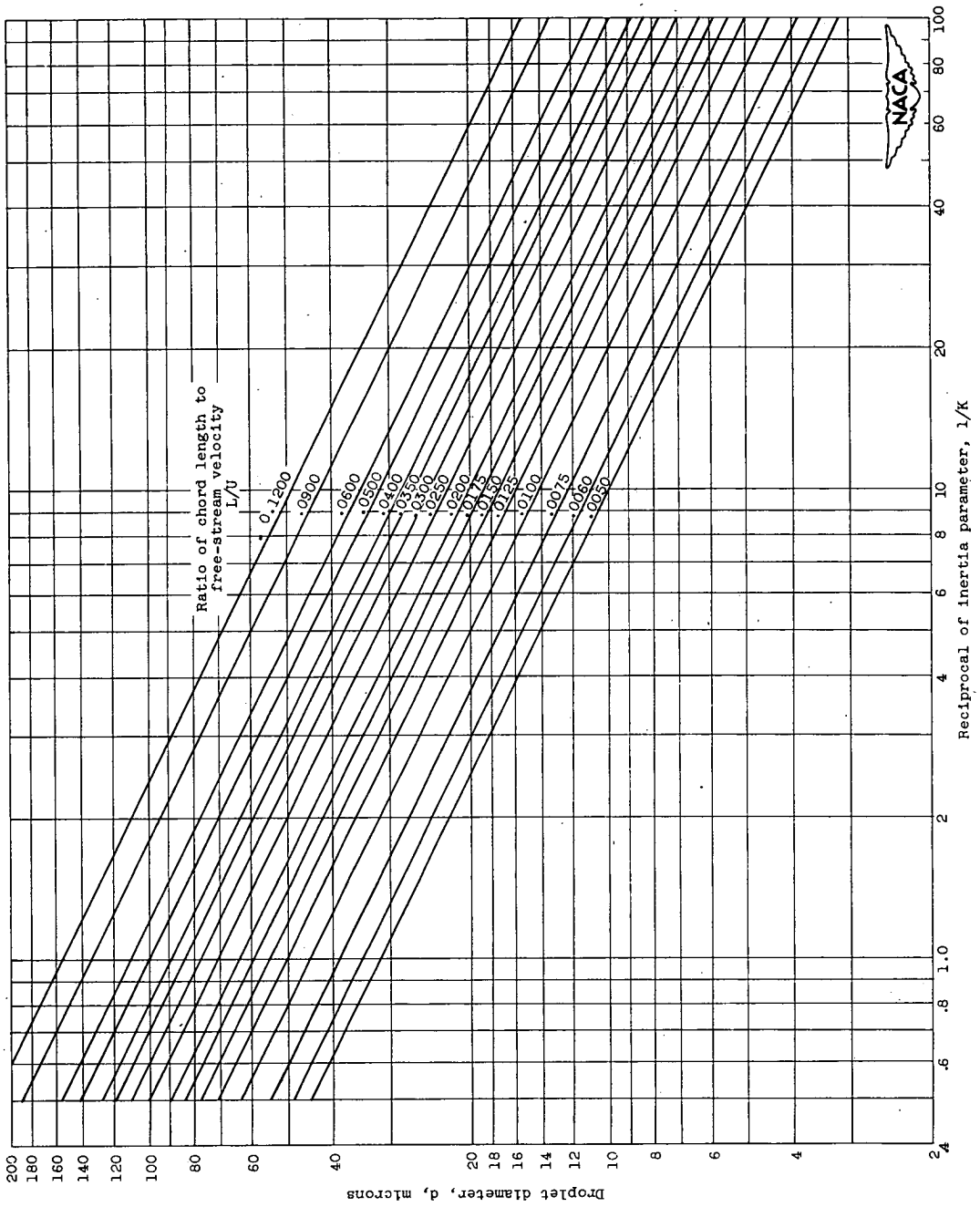

(a) Altitude, 10,000 feet.

Figure 12. - Droplet diameter as function of reciprocal of inertia parameter.

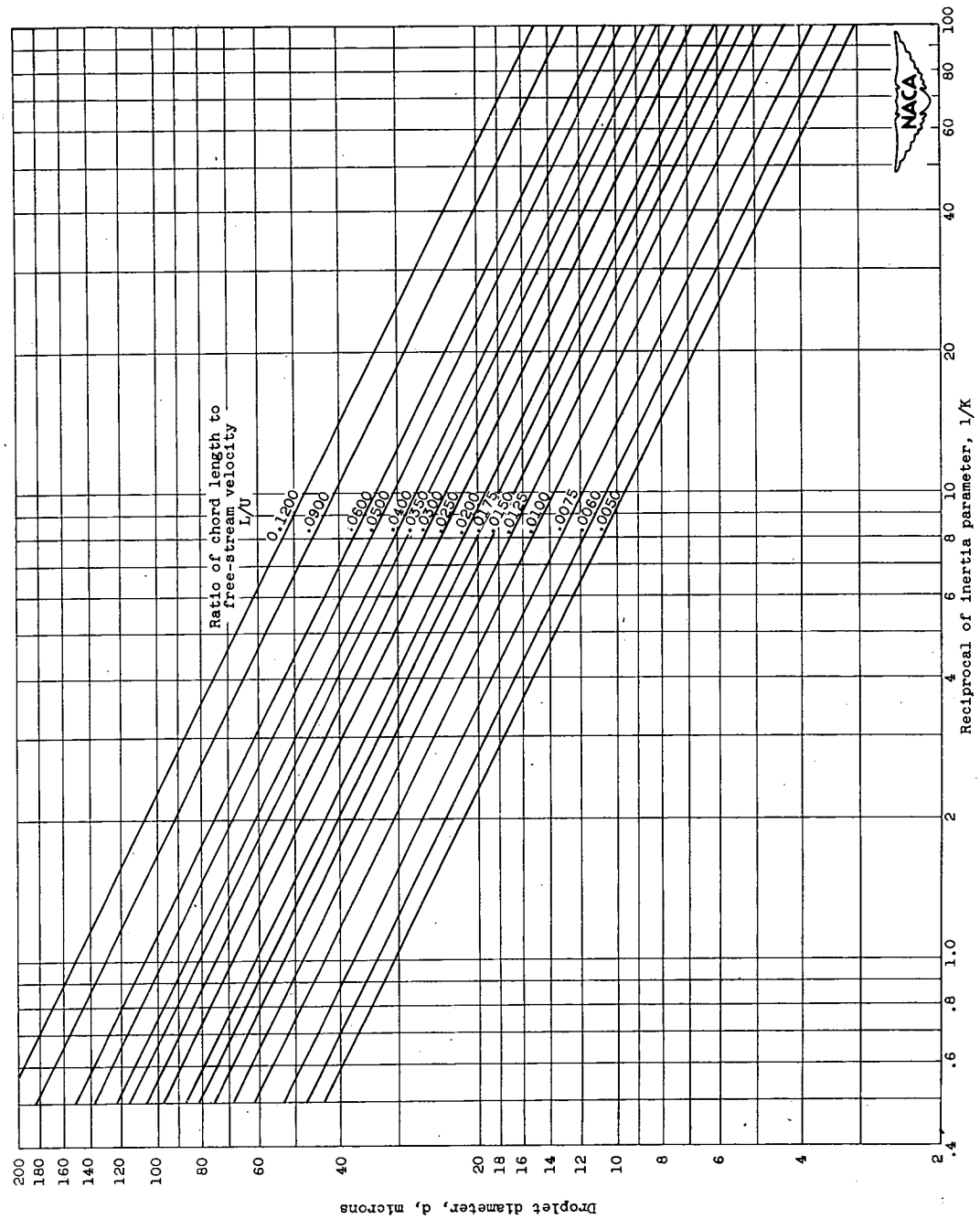

(b) Altitude, 30,000 feet.

Figure 12. - Concluded. Droplet diameter as function of reciprocal of inertia parameter.

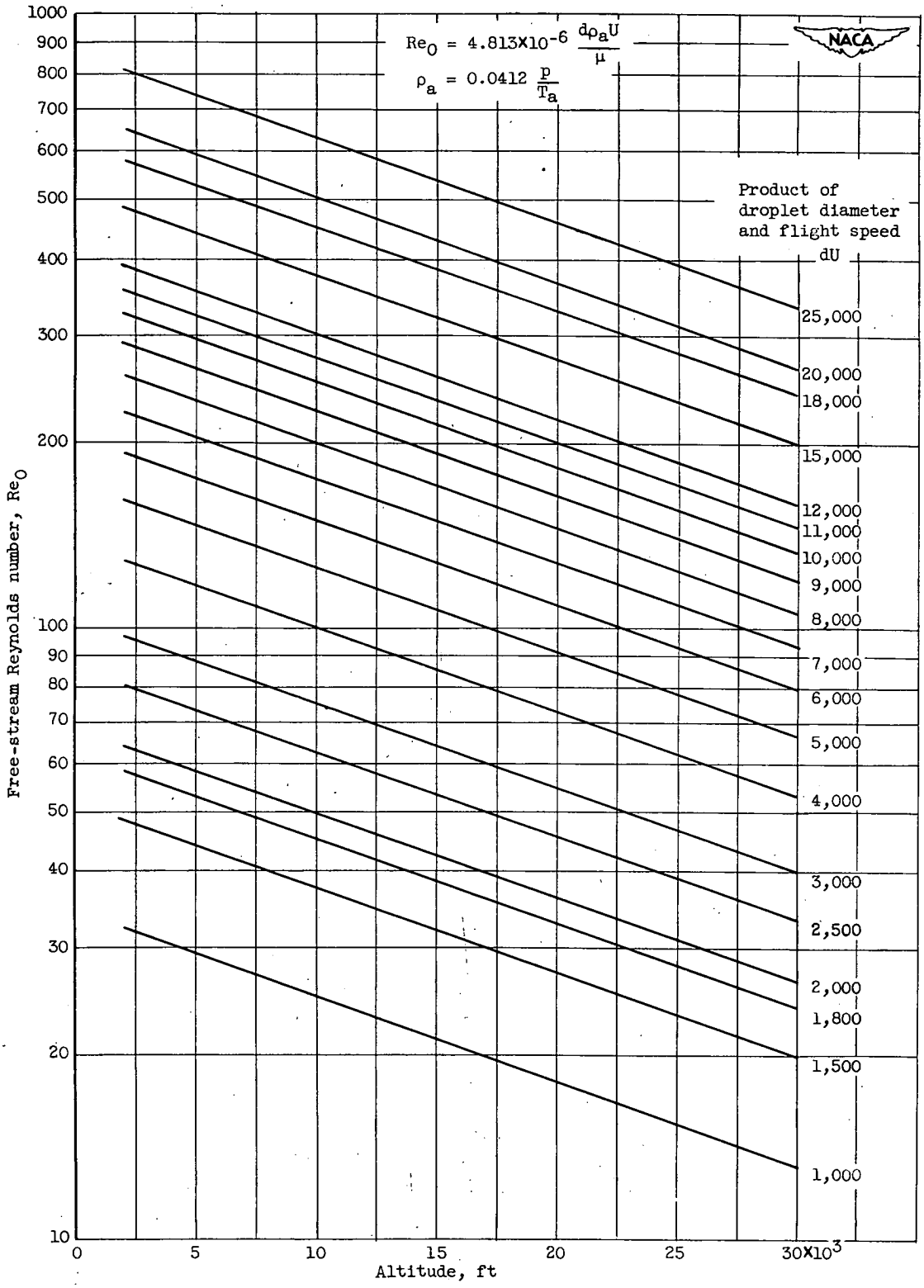

Figure 13. - Free-stream Reynolds number as function of altitude. (Units of U are mph.)

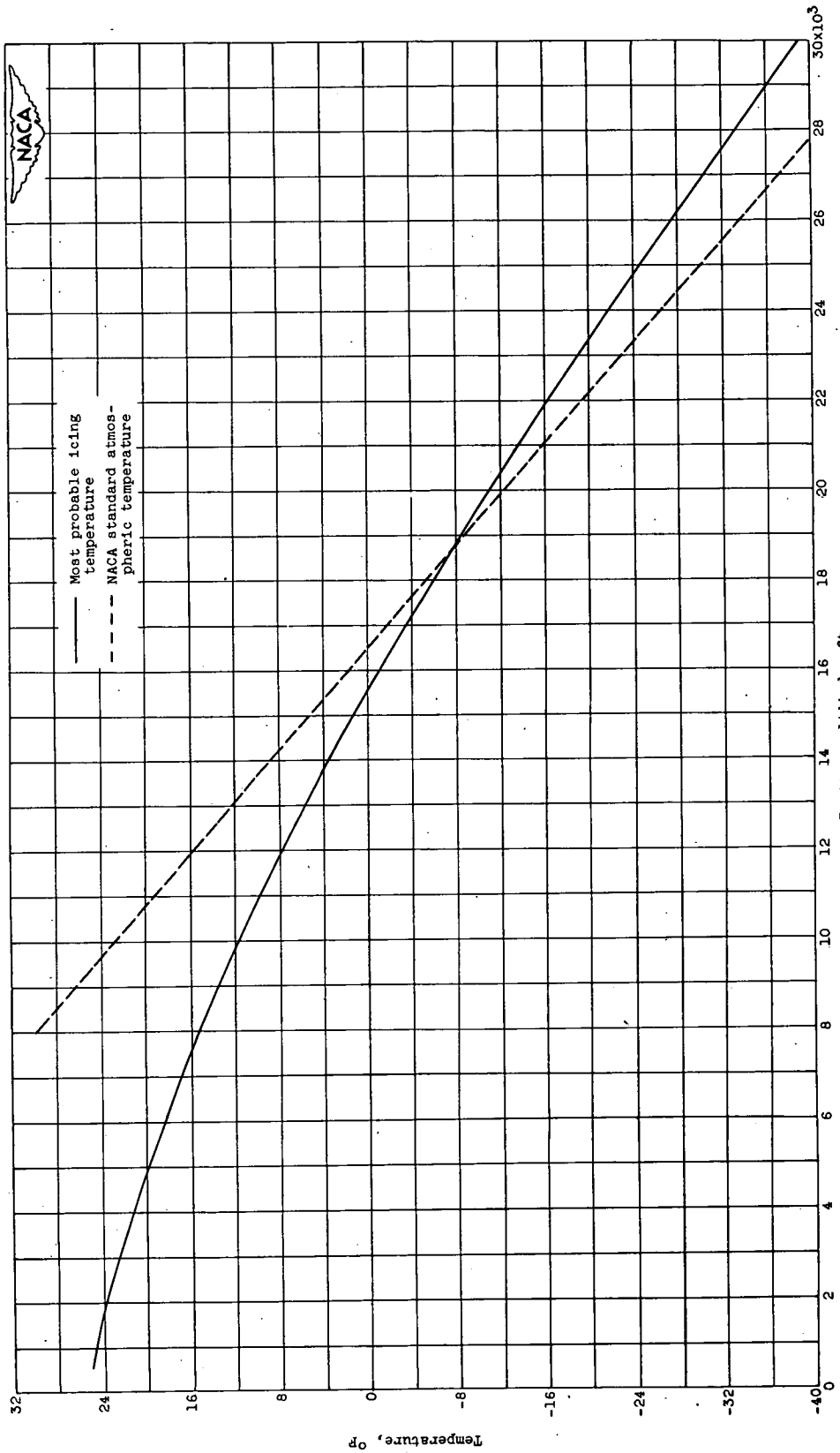

Figure 14. - Most probable icing temperature as function of pressure altitude. Most probable icing temperature at various altitudes obtained from approximately 300 icing observations (reference 7).

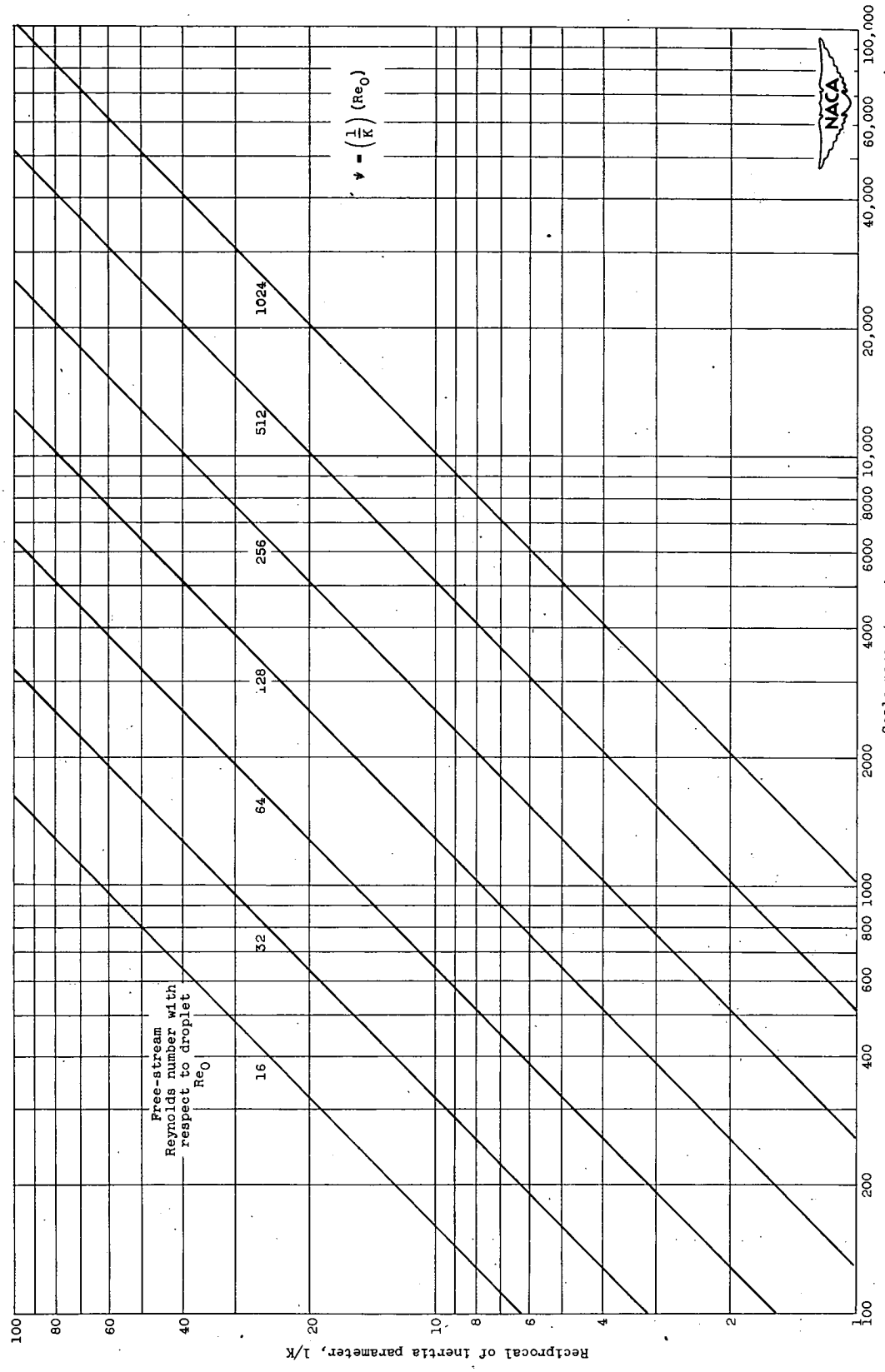

Figure 15. - Reciprocal of inertia parameter as function of scale parameter.

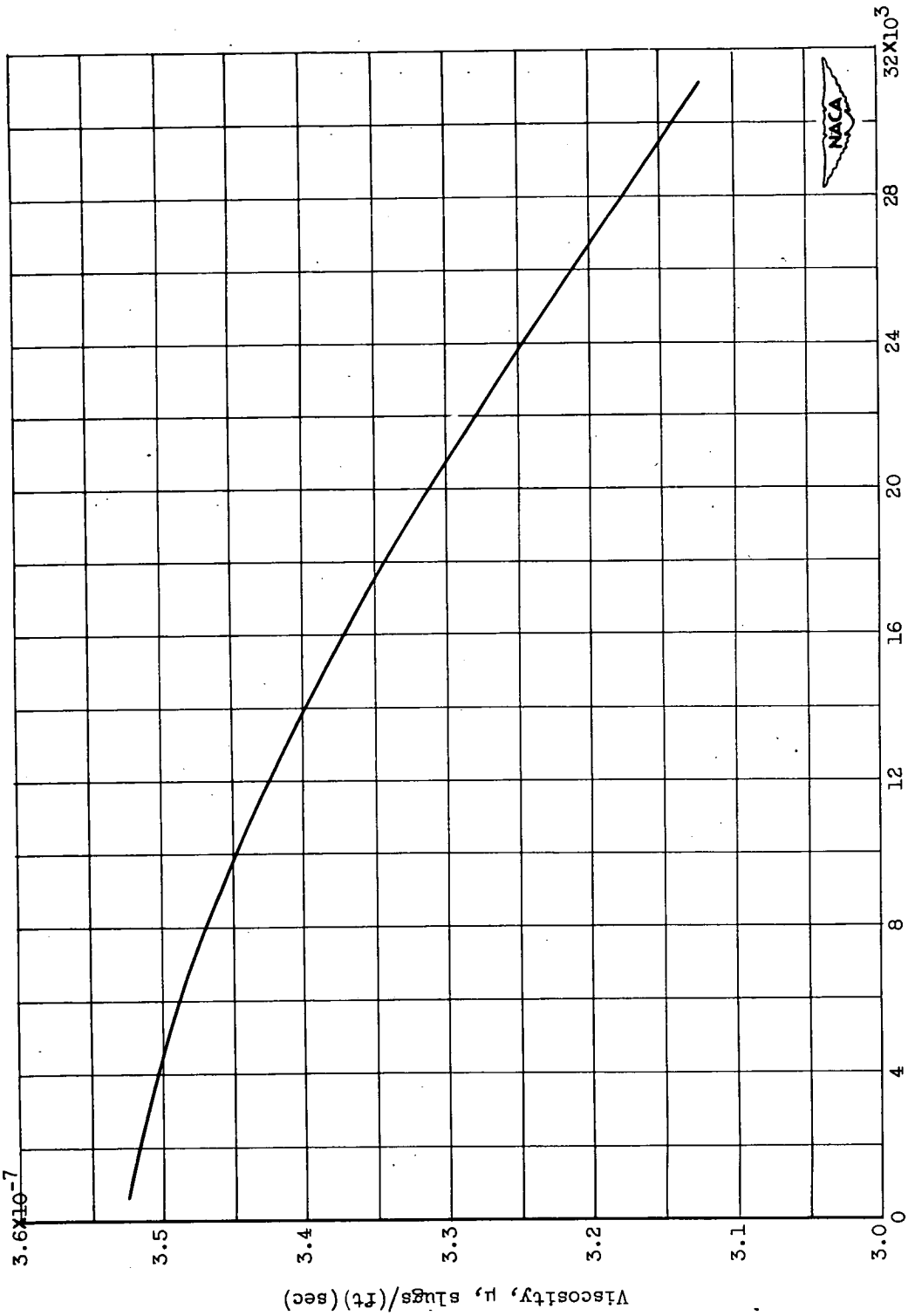

Figure 16. - Air viscosity as function of pressure altitude. Based on most probable icing temperature.